CORRELATION STUDY OF THE UNDERWATER DIFFRACTION PATTERN OF A CORRUGATED AIR-WATER INTERFACE

By J. G. Duffey, Jr.

Technical Memorandum
File No. TM 215.2221-05
July 25, 1968
Contract NOw 65-0123-d
Copy No. 23

The Pennsylvania State University
Institute for Science and Engineering
ORDNANCE RESEARCH LABORATORY
University Park, Pennsylvania

NAVY DEPARTMENT · NAVAL ORDNANCE SYSTEMS COMMAND

87

Abstract: This experimental investigation examines the underwater diffraction pattern of a corrugated surface insonified by a warbletone (wide band FM) acoustic source. Sound field data is obtained using a variable-level correlation system to measure the pressure amplitudes of the first two forward and back-scattered orders. These measurements are carried out primarily for frequencies near those for which the various scattered orders fail to appear e.g. near the "cut-off" frequencies.

Satisfactory agreement between theory and experiment is obtained relative to the locations of the

File No. 215.221-05
July 25, 1968
WLB:amm
Total Pages: 81
Total Figures: 32

Abstract (Continued): various scattered orders in the spectra. Measured amplitudes of the scattered orders are generally close to the predicted values although increasing discrepancy with theory is noted for increasing order. This effect is due primarily to the theoretical complications which arise from the use of comparatively severe corrugations. Deviations from theoretical predictions attributable to angle of source incidence show no general trend. Extinction of the scattered amplitudes occur consistently at slightly higher frequencies than calculated. It is not determined decisively whether the amplitudes attained zero or merely very small values at the cut-off frequency due to the practical limitations on signal-to-noise ratio of the measuring system. However, (relative) scattered order amplitudes less than 0.2 of the specular amplitudes of plane surface reflections is obtained even with the present comparatively unrefined electronic equipment.

TABLE OF CONTENTS

TABLE OF CONTENTS

LIST OF FIGURES

LIST OF FIGURES

CHAPTER I

INTRODUCTION

1.1 The Problem and Its Significance

To gain an insight into the complex process of sound scattering from the sea surface, scientists have resorted to laboratory experiments using model pressure release corrugations to approximate the actual sea surface. By reflecting sound pulses from these corrugations, they have measured the effect of certain surface parameters on the basic scattering mechanism. Use of stationary sinusoidal corrugations afforded the greatest simplification in studying the process; it was for this reason that Tamarkin and LaCasce investigated the scattering process using three different sinusoids.

The present study was motivated by the section of their paper in which they expressed a need for more detailed examination of the scattering process near cut-off. For a given angle of source incidence, the cut-off frequency is defined as the minimum frequency below which a given scattered order fails to propagate. At this frequency and

below, the scattered order represents an exponentially damped distortion of the wave field in a direction normal to the pressure release surface.

The objective of the present study was to use a new approach, a correlator technique, in investigating the scattered field (diffraction pattern) from a stationary sinusoid near cut-off.

In the present application, the variable level correlator provides a unique means of separating the scattered orders from a temporally and spatially continuous sound field. The investigation contributes further evidence to the validity of existing scattering theory and affords a comparison of similar experiments, employing the standard pulse technique. Having established the usefulness of this correlator system, its application to other areas of investigation appears promising.

1.2 Related Theoretical Studies

The first to treat the scattering problem, Rayleigh,[16] assumed that the scattered field consisted of a discrete set of plane waves travelling away from the surface (a specular reflection, plus forward and backscattered orders). However,

he was unable to solve the problem for other than normal incidence, and then only under the condition that both the surface and acoustic wavelengths were large compared to the corrugation amplitude. In 1955, Tamarkin and LaCasce[10] solved the problem for an arbitrary angle of incidence using the same approach and physical assumptions as Rayleigh.

In 1952, L. M. Brekhovskikh[3] solved the problem by evaluating the Helmholtz integral. In estimating a boundary value for the gradient of the reflected pressure, he assumed that at the corrugated surface an incident wave is reflected locally, as though it undergoes an ordinary specular reflection. As will be indicated below, this is a poor assumption in the low frequency region. He further assumes that the surface has a reflection coefficient that depends, through a complex phase factor, on the surface coordinates; i.e., on the distance from an arbitrarily selected reference plane. The validity of his solution also requires that overshadowing does not occur. (This condition is also necessary for the other theories discussed here.) Overshadowing results when the angle of incidence exceeds the angle between the normal to the $z=0$ plane and the tangent to the surface at the point of maximum slope.

The analysis of Carl Eckart[6] does not require the assumption of microscopic specular reflection (Brekhovskikh) in his approach to the problem. This represents a significant improvement, because an acoustic reflection is not governed by small roughnesses or corrugations, but rather by averaging over areas comparable to the wavelength. Thus, it is always a region of at least $\lambda/4$ by $\lambda/4$ that determines the reflection.[17] The wave is reflected as if the actual surface area were replaced by a plane at its mean distance from the reference plane. Eckart thus assumed that the surface was "not too rough" and could be locally approximated by a plane surface parallel to the $z=0$ plane.

The most recent contributor to the scattering theory, J. L. Uretsky,[19,20] solved the Helmholtz integral written in terms of Green's functions. He made no assumptions concerning either the sound source frequency or the geometrical parameters of the surface. Unfortunately, the method gives little insight into the practical application of the solution. However, Barnard, Horton, Miller and Spitznogle,[1] have recently presented an interesting paper on the practical aspects of the numerical computation of the results given by Uretsky.

Experimentally, American and Soviet scientists in the early 1950's investigated scattering from regular geometrical shapes and sinusoids. They measured the amplitudes, energies, beam widths, and directions of propagation of the various scattered orders.[10,11,15] In succeeding years, a shift to more random surfaces was made as theory became available. Based on the success investigators have had in explaining scattering from stationary sinusoidal and random surfaces, it seems probable that future emphasis will be directed to scattering from a time dependent random surface.

1.3 Objective of the Investigation

The purpose of this investigation was to measure the relative scattered pressure amplitudes near cut-off employing a variable level correlator system and warbletone source (FM) generator. Theoretically, finite cut-off amplitudes are predicted, but experimentally the cut-off behavior has not been resolved.

The investigation was performed subject to the following restrictions: First, the frequency range of the source was 20kHz to 100kHz, a range including the cut-off frequencies for the selected source alignments. Three source positions

were utilized: 0°, 10°, and 30°. These angles were measured between the axis of the major lobe of the projector and the vertical to the z=0 plane. Because of the above restrictions and the choice of the sinusoidal surface parameters, only a maximum of two scattered orders could be measured within the physical limitations of the underwater environment.

CHAPTER II

ECKART'S THEORY OF SCATTERING

2.1 Selection of the Method

Of the several theories briefly discussed in the first chapter, the most recent, by Uretsky, appears to be most accurate and mathematically sophisticated. However, because of the difficulty in the numerical evaluation of the scattered amplitudes (a computer is required), a method was selected that showed reasonable promise of yielding acceptable results without using numerical techniques.

Although the theories of Rayleigh, Brekhovskikh, and Eckart satisfy the above requirements, only Eckart's is suitable for the present study. Rayleigh's solution in closed form predicts neither a cut-off frequency nor scattered orders beyond the first, and Brekhovskikh indicates that the scattered amplitudes increase at cut-off in certain situations. Eckart's theory possesses none of these shortcomings and conforms to the experimental results of several investigations.[7,10] Therefore, the scattered amplitudes, relative to the specular amplitude from a plane surface, will be derived

following Eckart's method as applied to a sinusoidal surface by Tamarkin and LaCasce.[10] It is with their paper that the results of the present study will be compared.

2.2 Derivation of the Scattered Amplitudes

The approach used in deriving the amplitude of the m^{th} scattered order is to solve the Helmholtz integral by estimating the boundary value of the gradient of the reflected pressure and applying applicable boundary conditions, far field criteria, and a directional source. This method, known as the Kirchoff approximation, is discussed in most texts on radiation theory.[4,8] This approximation, more exact in the high frequency limit, assumes that the reflection from the corrugation can be approximated by that of a plane surface. Explicitly, the Helmholtz integral[2,4] may be written as

$$4\pi p_1(A) = \int_S \left\{ \partial p_1/\partial n_1 \; e^{ikr_1}/r_1 - p_1 \; \partial/\partial n_1 \; (e^{ikr_1}/r_1) \right\} ds_1 . \qquad (2.1)$$

In this expression the following should be noted:

(a) p_1 refers to the boundary value of the reflected pressure.

(b) All derivatives are to be evaluated on the surface, $z_1 = \zeta = h \cos(px)$, where h and p are the corrugation amplitude and wave number, respectively.

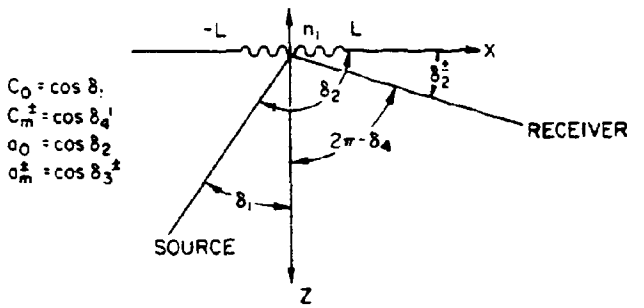

Figure 2-1. Eckart Theory Geometry (Angle Identifications)

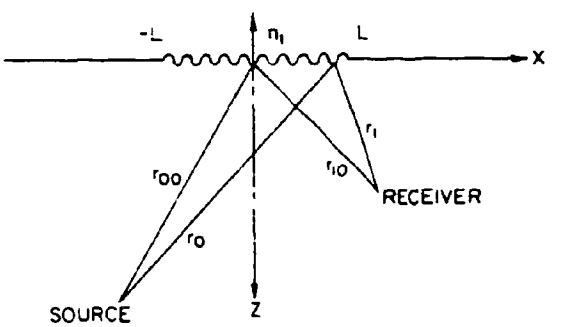

Figure 2-2. Eckart Theory Geometry (Distance Identifications)

(c) Since the surface corrugation is essentially along the x-axis, $ds_1 = dx_1$, and the limits on integration are the effective corrugation length, -L to L.

The incident pressure p_o is given by the following expression:

$$p_o = \frac{De^{ikr_o}}{r_c} \quad . \tag{2.2}$$

D will be required to be constant over the region of insonification and zero otherwise. Explicitly,

$$D(x) = D \quad \text{for} \quad |x| \leq L \tag{2.3}$$
$$= 0 \quad \text{otherwise} \quad .$$

Because the surface is assumed to be slowly varying ($hp << 1$),

$$\partial/\partial n_1 = - \frac{\partial}{\partial z_1} \quad . \tag{2.4}$$

To insure that both r_o and r_1 are much larger than the acoustic wavelength ($kr >> 1$), the corrugation must be placed in the far field of the source. The source and receiver distances from the surface were set at the same order of magnitude (see Figure 2-2). The following expressions are good approximations of these distances:

$$r_o \simeq r_{oo} - (a_o x_1 + c_o \zeta) \quad . \tag{2.5}$$

$$r_1 \simeq r_{10} - (a_m^+ x_1 + c_m^+ \zeta) \quad . \tag{2.6}$$

These equations are derived in Appendix A.

For a pressure release surface the following condition must be met at the surface:

$$p_1 = - p_o \text{ at } z_1 = \zeta \quad . \tag{2.7}$$

A value for $(\partial p_1/\partial n_1)$ is necessary to solve the Helmholtz integral, Equation (2.1). This value may not be arbitrarily assigned, as pointed out by several authors.[11,13] A knowledge of p_1 or $\partial p_1/\partial n_1$ at the interface is sufficient to completely specify the problem; hence, they cannot be independent. Unfortunately, there is no way of exactly determining $\partial p_1/\partial n_1$, as Equation (2.7) gives the only relation between p_1 and p_o. Thus, an approximation for $\partial p_1/\partial n_1$ is required if the problem is to be solved. Eckart's estimate assumes that the surface is "not too rough" and may be replaced by a plane surface.[14] The resulting expression is

$$\left.\partial p_1/\partial n_1\right|_\zeta = \left.\partial p_o/\partial n_1\right|_\zeta \tag{2.8}$$

Substituting Equations (2.7) and (2.8) into the Helmholtz integral, Equation (2.1) yields:

$$4\pi p_1(A) = \int_s \left\{ \partial p_o / \partial n_1 \left(e^{ikr_1}/r_1\right) - p_o \, \partial/\partial n_1 \left(e^{ikr_1}/r_1\right) \right\} ds_1$$

Substitution of Equation (2.2) further reduces the last equation to:

$$4\pi p_1(A) = \int D \, \partial/\partial n_1 \left[e^{ik(r_o + r_1)}/r_o \, r_1\right] \, ds_1 \qquad (2.9)$$

This may be simplified by performing the indicated differentiation and utilizing the far field assumption ($kr >> 1$), therefore

$$4\pi p_1(A) = \int (D/r_o r_1) \, \partial/\partial n_1 \left[e^{ik(r_o + r_1)}\right] \, ds_1 \; . \qquad (2.10)$$

Next, a value for $(r_o r_1)$ and $(r_o r_1)$ is needed. To the first order, Equations (2.5) and (2.6) yield:

$$r_o r_1 \approx r_{oo} r_{10}$$

and

$$r_1 + r_o \left(r_{oo} + a_o x_1 - c_o \zeta_1 + r_o - a_m^{\pm} x_1 - c_m^{\pm} \zeta_1\right)$$
$$= \left(r_{oo} + r_{10} - a x_1 - c \zeta_1\right) \; ,$$

where

$$a = a_o + a_m^{\pm} \quad \text{and} \quad c = c_o + c_m^{\pm} \; .$$

Substituting these last two expressions into Equation (2.10), along with Equation (2.4) gives

$$4\pi p_1(A) = \cdot D/r_{oo}r_{10} \int_{-L}^{L} \delta/\delta z_1 \left\{ e^{ik(r_{oo} + r_{10} - ax_1 - c\zeta_1)} \right\}_{L} dx_1,$$

$$4\pi p_1(A) = - ikcD/r_{oo}r_{10} \int_{-L}^{L} e^{ik(r_{oo} + r_{10} - ax_1 - c\zeta)} dx_1. \quad (2.11)$$

The reflected pressure from a finite length plane surface can be derived from Equation (2.11), if $\zeta = 0$. If that pressure is denoted by $p_o(A')$, then,

$$4\pi p_o(A') = ikcD/r_{oo}r_{10}\, e^{ik(r_{oo} + r_{10})} \int_{-L}^{L} e^{-ikax_1} dx_1 \quad (2.12)$$

$$= - Dc/a \left(e^{ik(r_{oo} + r_{10})}/r_{oo}r_{10}\right) [e^{-ikaL} - e^{ikaL}]$$

$$= 2ikLDc \left(e^{ik(r_{oo} + r_{10})}/r_{oo}r_{10}\right) \sin(kaL)/kaL ,$$

and finally,

$$4\pi p_o(A') = 4ikLMc_o \left(\sin(kaL)/kaL\right), \quad (2.13)$$

where $M = D\, e^{ik(r_{oo} + r_{10})} / r_{oo} r_{10}$.

and $c = c_o + c_m^{\pm} = 2c_o$.

for a specular reflection (see Figure 2-1).

Equation (2.13) is the reference pressure to which $p_1(A)$ will be compared.

Rewriting Equation (2.11), expressing ζ explicitly gives

$$4\pi p_1(A) = Mick \int_{-L}^{L} e^{-ikax_1} e^{-ikch \cos(px_1)} dx_1 . \qquad (2.14)$$

This integral is most easily evaluated by using the identity

$$e^{-ikch \cos(px)} = [\, J_o(-kch) + 2iJ_1(-kch)\cos(px) - \ldots .]$$

Retaining only the first two terms of the identity, Equation (2.14) becomes

$$4\pi p_1(A) = Mick \left[\int_{-L}^{L} J_o(-chk)\, e^{ikax_1} dx_1 + 2i \int_{-L}^{L} J_1(-chk)\cos(px) e^{-ikax_1} dx_1 \right]. \qquad (2.15)$$

The first integral represents the contribution to the scattered pressure of the specular reflection from the finite corrugation. The second integral is the contribution of the first scattered order. The first integral can be solved as was Equation (2.12).

As a result, the specular contribution is

$$4ikLMc_o \ (\sin(kaL)/kaL) \ \ J_o(-2c_o hk). \qquad (2.16)$$

Evaluation of the second integral is obtained from standard integral tables. The final result, after supression of the factor "i", is

$$[4ckMJ_1(-chk)/(p^2-k^2a^2)] \ [p\sin pL \cos(kaL) - ka \cos pL \sin(kaL)]. \qquad (2.17)$$

Equation (2.15) may now be written as:

$$4\pi p_1(A) = [4ikLMc_o(\sin(kaL)/kaL) \ J_o(-2c_o hk)] + [4ckMJ_1(-chk) /(p^2 - k^2a^2)] \ [p\sin pL \cos(kaL) - ka \cos pL \sin(kaL)] . \qquad (2.18)$$

The desired expression, $p_1(A)/p_o(A')$, can be calculated. This expression is the ratio between the sum of the scattered amplitudes and the specular reflection amplitude from a plane surface. In principle, this ratio will contain an infinite number of terms, one for each scattered order present. In the present derivation, only the first (zero or specular order) and second (first order) terms are retained. The first term is the ratio between the specular amplitudes of the corrugation, [Equation (2.16)] and the plane surface [Equation (2.13)] and is called the "relative" specular amplitude A_o:

$$A_o = J_o(-2c_o hk) \ . \qquad (2.19)$$

The "relative" first scattered amplitude, $A_1^{\pm}$, is obtained from the ratio of Equations (2.17) and (2.13). The $(^{\pm})$ superscript refers to the direction of propagation of the first scattered order, and is (+) in the forward direction and (-) in the backward direction. Forward scattering occurs when the direction of propagation is between the positive x-axis and the specular direction for a source positioned as depicted in Figure 2-1. Explicitly, the ratio becomes

$$A_1^{\pm} = c_o + c_{1/c_o}^{\pm} [kaL/\sin(kaL)]\, J_1(-chk)\, [p\sin(pL)\cos(kaL) - ka \cos pL \sin(kaL)/L(p^2 - k^2a^2)] \quad . \tag{2.20}$$

note, $c_m^{\pm}$ becomes $c_1^{\pm}$

This expression may be simplified by a useful limiting technique. The grating equation for the first scattered order is:

$$p = \pm ka \tag{2.21}$$

For the present purpose, it may be rewritten as:

$$p = \lim_{\epsilon \to 0}^{+} (ka + \epsilon) \tag{2.22}$$

Neglecting higher order terms, Equation (2.20) becomes:

$$A_1^{\pm} = \lim_{\epsilon \to 0}[(c_o+c_1^{\pm})/2c_o][J_1(-chk)/\sin(kaL)]\{ka\cos(kaL)[\sin(kaL)\cos(\epsilon L) + \cos(kaL)\sin(\epsilon L)] + \cos(kaL)[\sin(kaL) + \cos(kaL)\sin(\epsilon L)] - ka\sin(kaL)[\cos(kaL)\cos(\epsilon L) - \sin(kaL)\sin(\epsilon L)]\}.$$

Taking the indicated limit for a corrugation with an integral number of surface wavelengths effective in the scattering process, we have:

$$A_1^{\pm} = c_o + c_1^{\pm}/2c_o \; J_1[-(c_o + c_1^{\pm})\, hk] \; . \qquad (2.23)$$

Even for a corrugation with a non-integral number of surface wavelengths, this result is essentially correct. Contributions to the scattered pressure from the outer edges of the corrugation will be relatively small, regardless of the phase difference between the two edges. This is especially true for a long corrugation length.

Higher order scattered amplitudes are calculated in the same manner as $A_1^{\pm}$; the general result is:

$$A_m^{\pm} = [c_o + c_m^{\pm}/2c_o]\; J_m[-(c_o + c_m^{\pm})\, hk] \; , \qquad (2.24)$$

where m is the scattered order of interest. Only the magnitude of these amplitudes is used in this study.

CHAPTER III

INVESTIGATION PROCEDURE

3.1 Apparatus

3.1.1 Variable Level Correlator. The basic problem in measuring the scattered amplitudes from a continuous source is separating the scattered signal from both the direct source signal and the multiply reflected signal (reverberant field). A variable level correlator designed and tested by J. Macaluso[12] was chosen as the solution to the problem because it provided both phase and amplitude correlation information on the transmitted and received signals.[4]

As indicated in Figure 3-1, a signal generator feeds an amplified signal to both a projecting transducer and a summing amplifier, where the source signal is combined with the signal from a ramp (saw tooth) generator (a signal with a uniform amplitude distribution, i.e., every amplitude is equally probable). This combining operation is the feature which permits amplitude information to be retained by the

correlator, in spite of the clipping operations performed later by the digital processor. Qualitatively, the summing operation produces an amplitude weighted signal. The same function is simultaneously performed on the received signal. The outputs of the summing amplifiers are then fed to zero axis crossing detectors, which detects positive and negative voltage excursions--the resulting wave form appears as a square wave of variable period. The zero-axis crossing detector is converted into a variable level axis-crossing detector when applied to the summed signal by effectively replacing the zero axis by the variable ramp voltage. Excursions about the ramp are thus detected. From this point on, the amplitude information is retained implicitly in the clipped signal's phase.

To account for the propagational time delay of the received signal, a digital shift register delays the transmitted signal in channel "A" so that the two signals have been delayed by the same amount of time before entering the phase comparator. Any subsequent change in the length of the signal path in water will appear as a time shift between these signals--a parameter that the correlator is capable of measuring. The initial time delay is set equal to the central beam transit time of the transmitted signal in reaching the

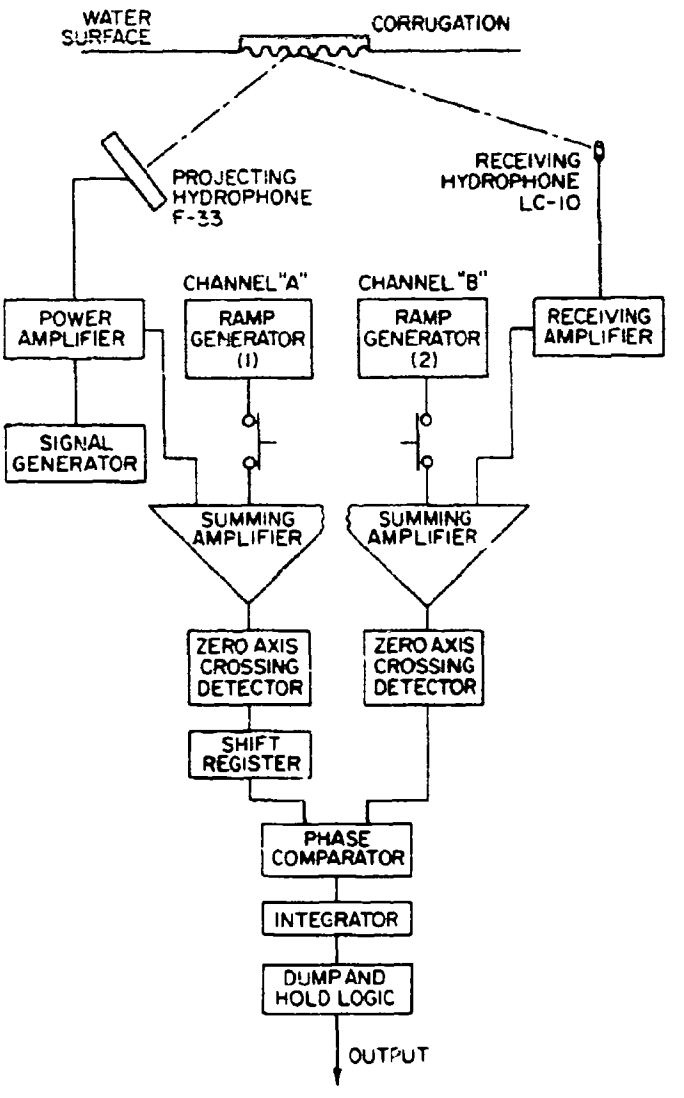

Figure 3-1. Variable Level Correlator System Schematic

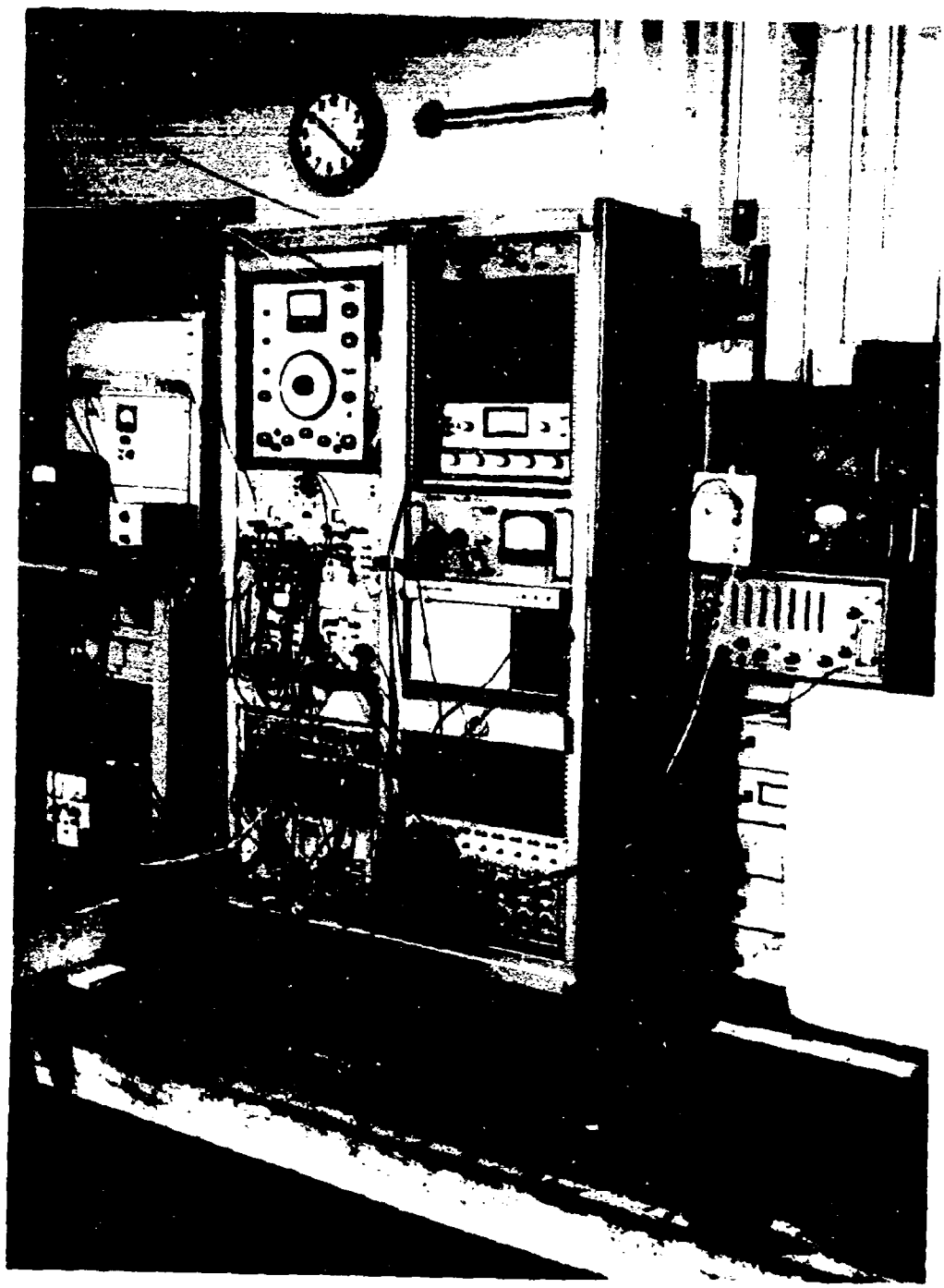

Figure 3-2. Variable Level Correlator System

receiver along the specular path. Delays ranging from 0.8 msec. to 4.6 msec. are introduced by adjusting the frequency of the clock generator which triggers the shift register.[12]

Output samples of the two channels are combined in a phase comparator, and the result is integrated. It is important that the two ramp signals have a zero (or nearly zero) cross-correlation function. This is implemented by generating ramps with incommensurate periods. The result of successive integrations is stored in a capacitor, the voltage of which indicates the degree of correlation at that instant. With the ramps disconnected, the processor functions as a clipper correlator (phase correlator); in this mode, the output of the correlator has the following interpretations:

(a) An output voltage of 5.6 volts indicates perfect correlation (in phase condition);

(b) A voltage of zero indicates an uncorrelated condition (random phase);

(c) A voltage of -5.6 volts indicates the 180° relative phase condition--"anti-correlation."

By connecting an x-y recorder to the output of the correlator and traversing the tank slowly with the receiver

(at a depth fixed and corresponding time delay), a spatial correlation function can be obtained. Figure 3-2 shows the actual correlator system.

To utilize this device one must determine the relationship between the correlator output and the signal strength measured at the receiver. Figure 3-3 presents a calibration curve valid for source frequencies extending from about 20kHz to 120kHz. The graph was obtained by progressively reducing the received signal level at the position of maximum correlation on the direct beam (for a fixed delay).

3.1.2 Receiving System. A small LC-10 omnidirectional hydrophone (see Appendix C) was selected for the receiver because it minimized the spatial averaging of the received signal. It was also necessary to separate the hydrophone a suitable distance from the traverse beam to prevent the receiver from being partly shielded (Figure 3-4).

The traverse assembly was operated either manually or automatically by a pulley system. By attaching the slide of a variable resistance potentiometer to the pulley assembly and using the output voltage of the potentiometer to drive the x-channel of the x-y recorder, the horizontal position

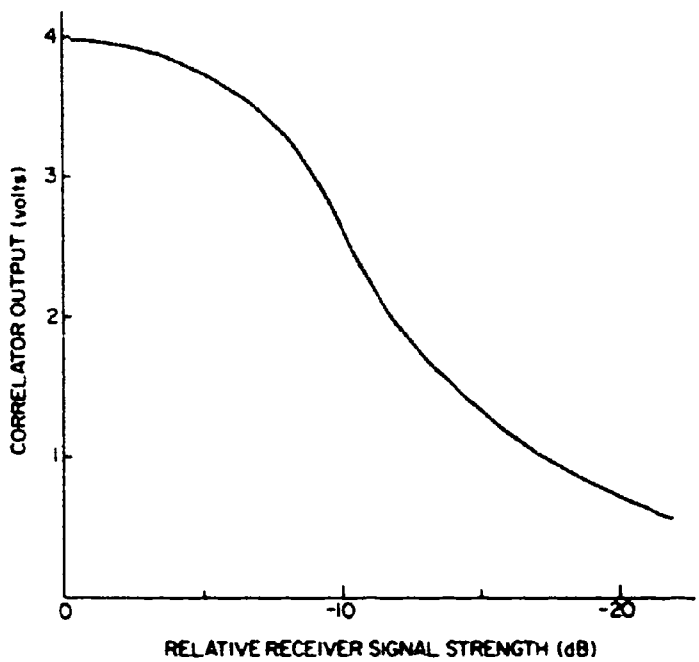

Figure 3-3. Correlator Calibration Curve

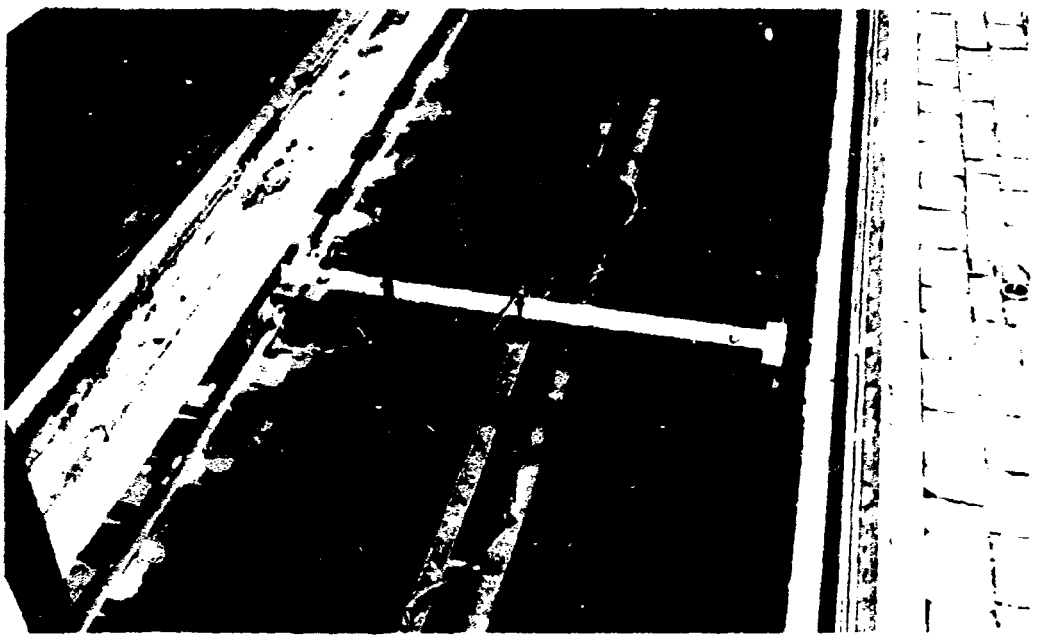

Figure 3-4. Transmitting and Receiving System (without Pressure Release)

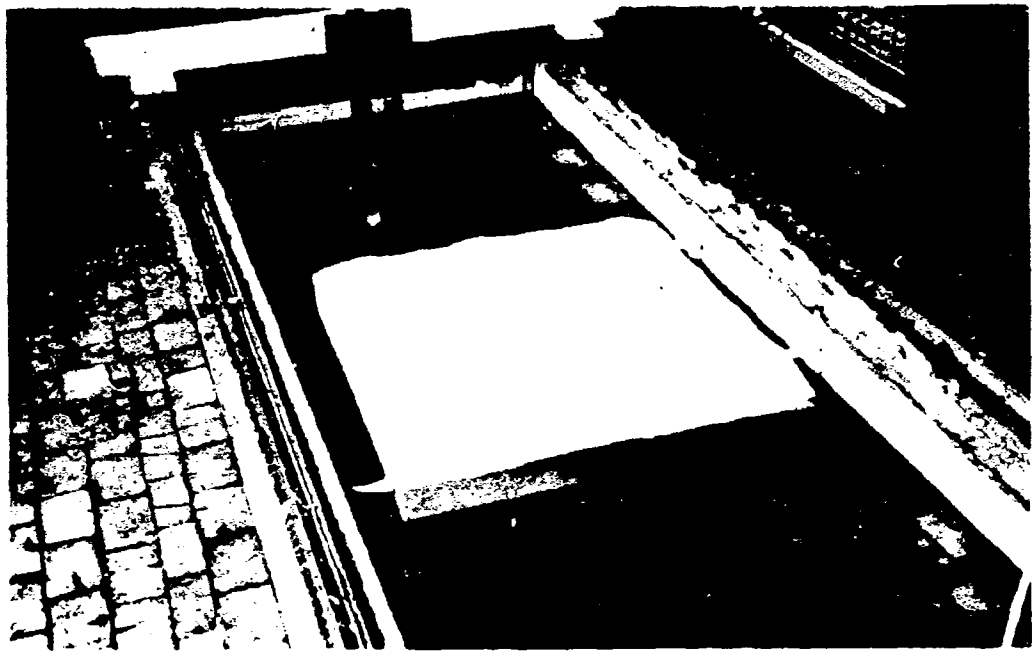

Figure 3-4. Transmitting and Receiving System (with Pressure Release)

of the receiver could be accurately determined. In addition, two photocells were attached to the frame at known locations. When tripped by lights on the wheel assembly, the correlator and x-y recorder were automatically disconnected thus providing an initial and final reference point for each traverse. The depth of the receiver was adjusted by another pulley assembly attached to the traverse frame. It was necessary to correct depth measurements for a half inch catenary found in the frame.

3.1.3 Other Apparatus. The projecting transducer, a USRD TYPE F-33, consisted of two co-axially mounted arrays (see Appendix C). The inner array measured approximately two inches square and had a useful frequency range extending from 5kHz to 150kHz. At the half power points the total beam width given was 12° at 150kHz.

Using the equation for a radiating piston, the beam width at the half power points should be approximately 18° at 100kHz and 45° at 35kHz.[12] Both arrays operating in parallel produced a much narrower beam ($7\ 1/2^{\circ}$ at 50kHz), but reduced the maximum useful frequency to about 50kHz. Because the correlator was found insensitive to beam width, the inner array was used exclusively. Far field conditions were insured by placing the projector at a depth of 66 inches.

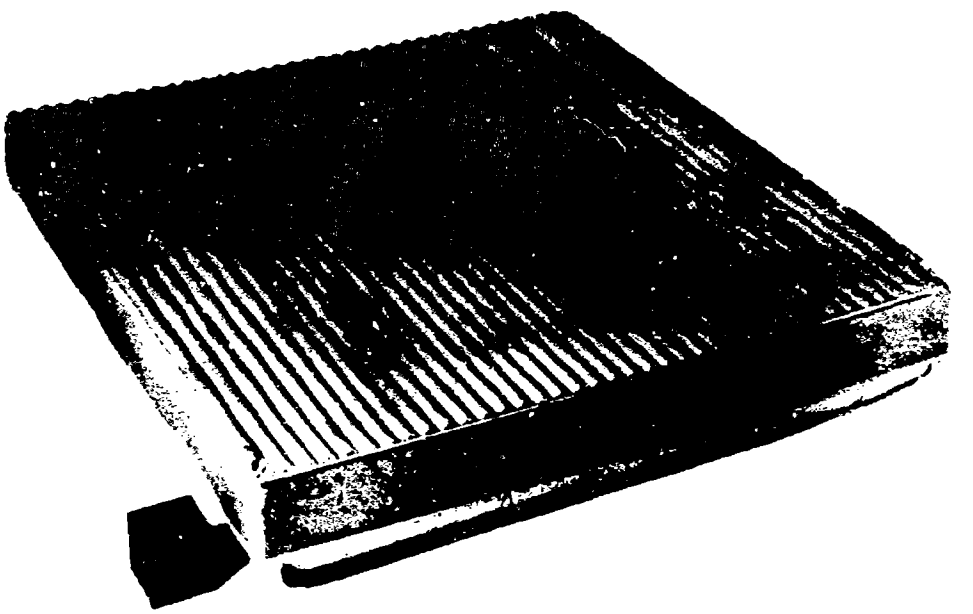

Figure 3-5. Pressure Release Corrugated Surface

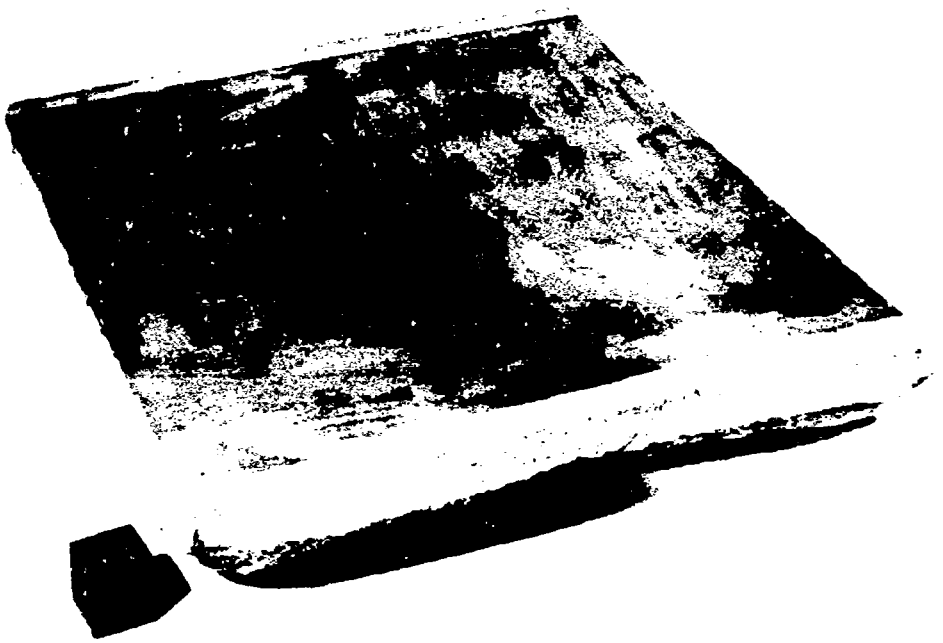

Figure 3-5. Pressure Release Plane Surface

In this experiment, the transducer used a wide band FM signal (warbletone). The carrier frequency was ramp modulated to produce a 2000 cycle swing to either side of the center frequency at a rate of 64 cycles per second.

To construct the pressure release reflecting surface, a special cutting tool was utilized to the desired corrugation into a piece of maple measuring 38-1/2" x 38-1/2" x 1". After mounting the corrugation in a frame, a urethane foam manufactured by the Armstrong Cork Company was applied to the surface by a frothing process. The frame was separated from the rigid urethane foam, after allowing it to cool (Figure 3-5). This substance, called Expandoform, had a density about ten times less than cork and was not water absorbent. The surface wavelength was 2.7 cm and the corrugation amplitude was 0.24 cm.

3.2 Procedure

With the flat surface in place, the projector was manually set at the desired angle of incidence. The scattered pressure was measured at points equally distant from the center of the corrugation (i.e., along the arc of a circle). After

computing the required time delay, a traverse was made at the proper depth to intercept the specularly reflected beam on the arc. The location of the resulting correlation function maximum provided an accurate indication of the source inclination.

With the flat surface replaced by the sinusoid, measurements of the scattered orders were made in essentially the same way. Using the grating Equation (4.1) as a guide, several traverses at constant depth were made, using frequencies surrounding the calculated value. The selection of the best trial was based on the position, maximum amplitude, and shape of the obtained correlation functions. By repeating this procedure for a number of depths, the dependence of the "relative" scattered amplitudes on frequency could be compared with theory.

In measuring both the scattered orders and the specular reflection from the plane surface for a given frequency, all system parameters were maintained constant, so that a valid comparison was possible. To avoid erroneous correlator indications, it was necessary to insure that the receiver was not overdriven. This occurred for certain receiver positions for projector input signals exceeding about 5 volts.

For this reason, the maximum projector input was arbitrarily fixed at 3.1 volts. The correlator inputs were always limited to about 1.5 volts.

CHAPTER IV

RESULTS AND CONCLUSIONS

4.1 Scattered Order Propagation

Before examining the scattered amplitudes, a comparison between the measured directions of propagation of the scattered order and the directions predicted by the grating equation will be made. For this purpose Equation (2.21) may be rewritten more clearly as follows:

$$\cos\delta_j^{\pm} = \sin\theta_i \pm m\lambda/\lambda_s \,, \tag{4.1}$$

where $\delta_j^{\pm}$ is the angle between the direction of propagation of the m^{th} scattered order and the positive x-axis (as illustrated in Figure 2-1), and θ_i is the angle of incidence measured from the normal to the z=0 plane. The order is given by "m", and λ/λ_s is the ratio of the acoustic wavelength to the surface wavelength. The positive sign denotes forward scattering; the minus sign, backscattering. For a fixed source angle, Equation (4.1) shows that a given scattered order starts out at grazing angle at the cut-off frequency but as the frequency increases, the angle approaches that of specular reflection.

Figures 4-1 and 4-2 compare theoretical and experimental propagational directions for the first and second orders. As the theory predicted, the scattered order propagates along the interface ($\delta_3^+ = 0$, $\delta_3^- = 180$) at cut-off. For frequencies below cut-off, $\delta_3^{\pm}$ becomes imaginary; thus, propagating spectra cannot be generated.

Both graphs agree consistently with theory (solid line); deviations are generally less than 2°. No forward scattered first order is found for a 30° angle of incidence. Similarly, there was no forward or backscattered second order for an incident angle of zero degrees. These results agree with the grating equation. Figures 4-3 and 4-4 depict the relationship between the cut-off frequency and incident angle for the first order. Although agreement is generally good, the experimental values are consistently greater than the predicted values. Figures 4-2 and 4-4 show somewhat larger deviations between data and theory for an angle of incidence of 30° than for 10°; however, for the first scattered order, deviations between data and theory show little dependence on angle of incidence (Figures 4-1 and 4-3). The high accuracy of these measurements establishes the suitability of this

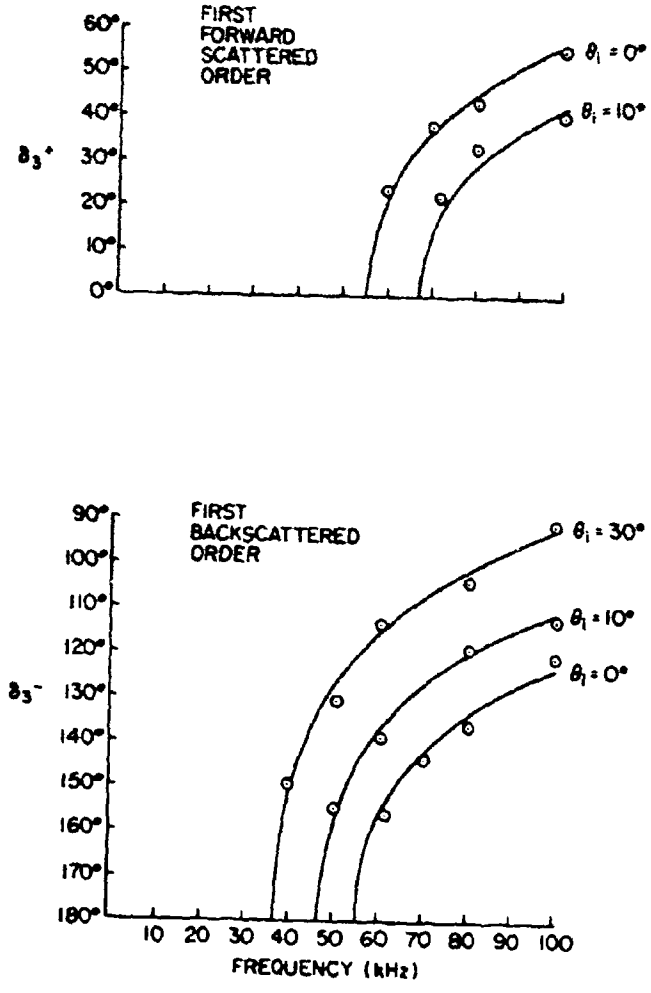

Figure 4-1. First Scattered Order Propagational Directions

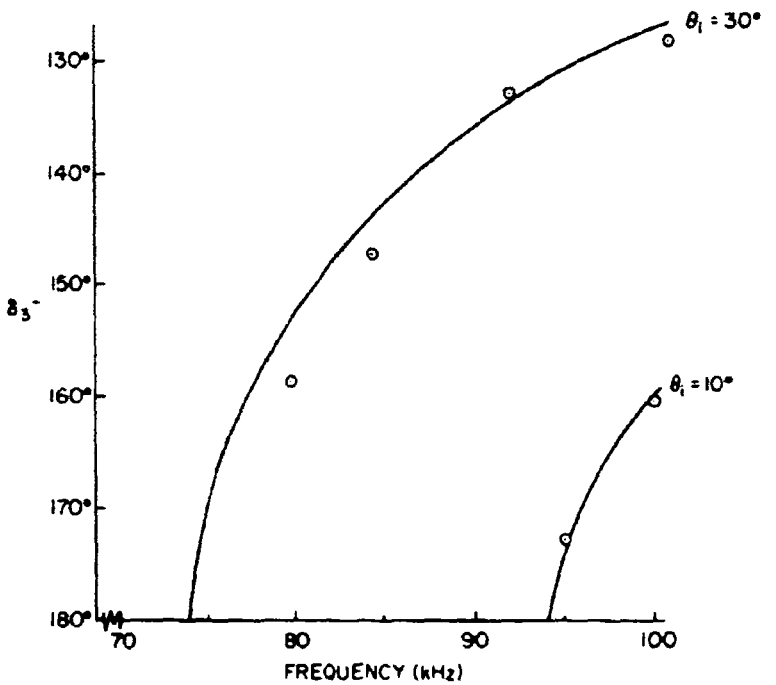

Figure 4-2. Second Backscattered Order Propagational Directions

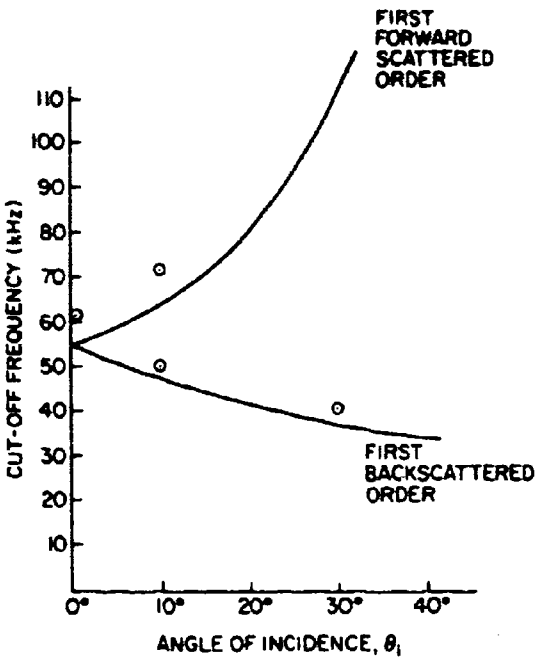

Figure 4-3. First Scattered Order Cut-Off Frequencies

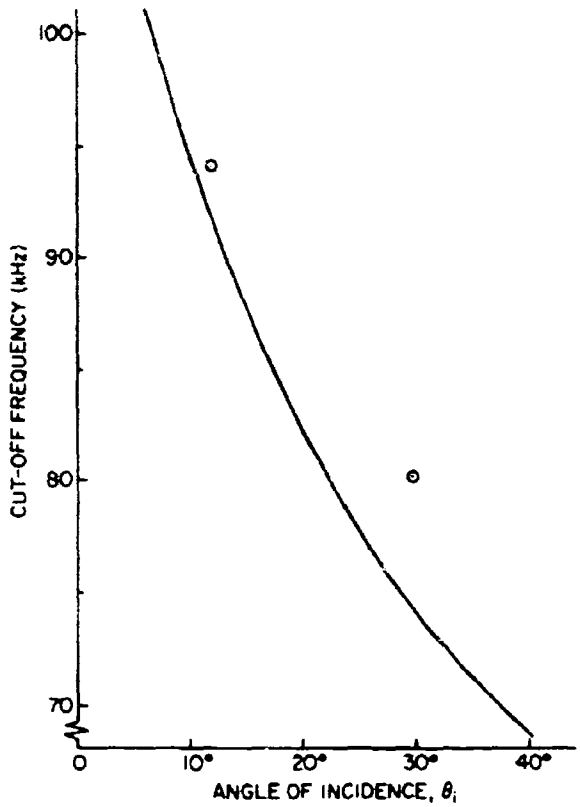

Figure 4-4. Second Backscattered Order Cut-Off

correlator technique for the present purpose. Furthermore, the correlator method permits use of a smaller laboratory tank than would be required in performing a similar experiment with the pulse-technique.

4.2 Scattered Order Amplitudes

In measuring the relative scattered amplitudes, it is necessary to determine the relationship between the correlator output and the scattered amplitude. A two-step procedure was used. The equation relating the sound pressure level (expressed in dB) and the signal amplitude level with respect to a fixed reference level is given by:

$$P = 20 \log A/A_{ref} \tag{4.2}$$

This experiment required two such expressions, one for the specular amplitude A_o, and one for the scattered amplitude A'. Thus,

$$\left\{ \begin{array}{l} P_o = 20 \log A_o/A_{ref} \\ P' = 20 \log A'/A_{ref} \end{array} \right\} , \tag{4.3}$$

where, P_o and P' are the pressure levels corresponding to A_o and A', respectively. P_o and P' are then obtained from the

calibration curve (Figure 2-3), which relates the correlator output to the relative receiver signal strength. Combining Equation (4.3) yields:

$$P_o - P' = \Delta P = 20 \log A_o/A' \qquad (4.4)$$

and

$$A'/A_o = A_m^{\pm} = [\text{ anti log } (\Delta P/20)]^{-1}. \qquad (4.5)$$

Here A'/A_o is the "relative" scattered amplitude as was computed by Equation (2.24).

Thus, by measuring the maximum amplitude of the correlation function, by applying the calibration curve, and by using Equation (4.5), the scattered signal can be determined.

4.2.1 Specular Amplitude A_o. The specular amplitude A_o, given by Equation (2.19), represents the ratio of the specular reflection from the corrugation to the reflection from a plane surface. Figures 4-5, 4-6 and 4-7 illustrate graphically the comparison between the experimental data and the theory for the three incident angles used. The surface used in the present study is intermediate in slope to surfaces two and three used in the Tamarkin and LeCasce investigation.[10] Their results agree closely with the corresponding measurements of this experiment. Agreement with theoretical

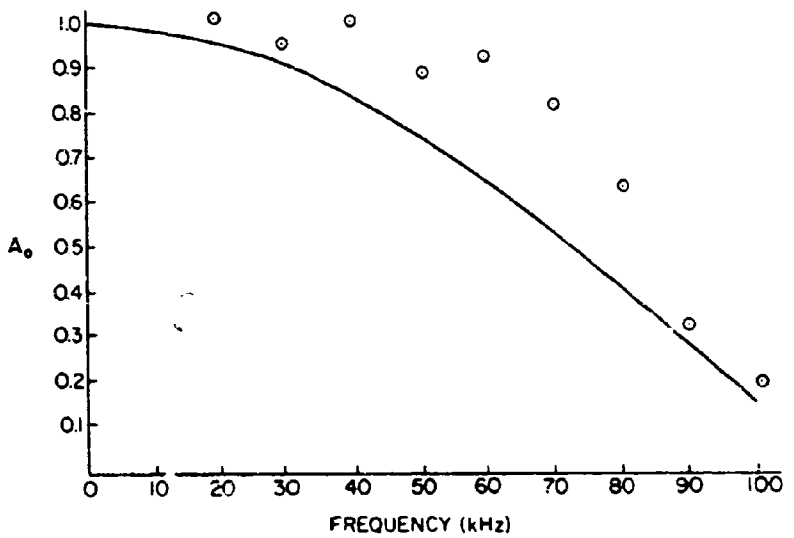

Figure 4-5. Specular Amplitude A_o for $\theta_i = 0^o$

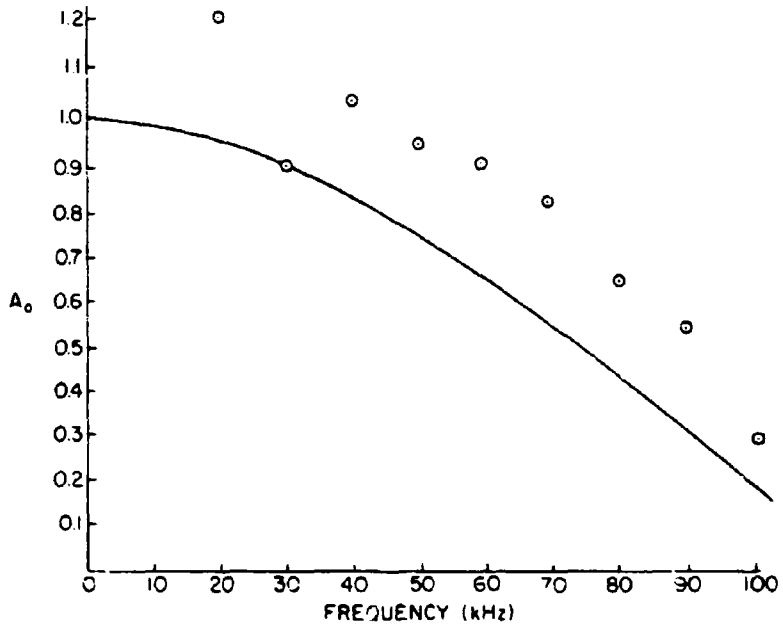

Figure 4-6. Specular Amplitude A_o for $\theta_i = 10^o$

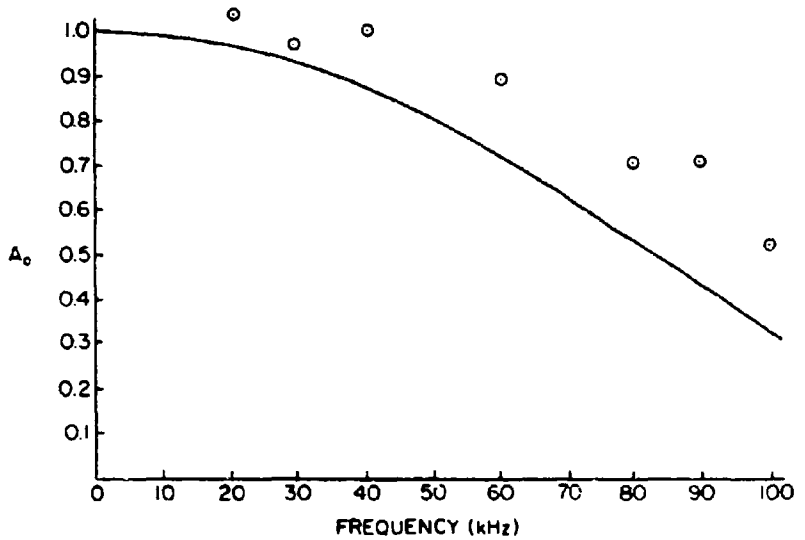

Figure 4-7. Specular Amplitude A_o for $\theta_i = 30^\circ$

values is particularly good at the high frequencies and for small angles of incidence. It is under these two conditions that Eckart's demand for local flatness is best satisfied. The criterion of local flatness when applied to those portions of the surface with least radius of curvature is given by the inequality:[10]

$$\cos\theta_i >> \pi h\lambda/\lambda_s 2 \quad .$$

4.2.2 First Scattered Order Amplitudes. The measured amplitudes of the first scattered order agree well with theory, especially at frequencies just above cut-off (see Figure 4-8 through 4-11). While cut-off usually occurred near the predicted value, determination of cut-off was inferred from the large positive slope manifested by the experimental data in the immediate vicinity of cut-off. However, the amplitudes of the first scattered order approached the cut-off frequency more rapidly than theory indicated, and they appeared to be extinguished at frequencies higher than predicted. Angle of incidence did not appear to be a very significant factor.

It was not definitely established whether the amplitude of the first scattered order is zero[2] or finite at cut-off. No relative amplitude below 0.18 was measured for this order, possibly due to the limitation placed on the system by its signal-to-noise ratio. The ambiguity at cut-off could be solved by employing a correlator system with better resolving power, and by using the projector at a higher incidence angle. (The theory indicates that the cut-off value of the scattered amplitude increases with increasing angle of incidence for forward scattered orders.)

In any event, the onset of the first scattered order was very sudden. For frequencies just below the achieved cut-off, no correlation function pattern was observed (see Figure 4-19), even with the ramps removed. Disconnecting the ramp generators converts the system into a clipper correlator, which is sensitive only to the relative phase between the two signals. The results obtained for the first scattered order extend upon the work done by Tamarkin and LaCasce by examining the frequencies in the immediate vicinity surrounding cut-off. Still, the behavior of the scattered amplitudes at the cut-off frequency is not answered decisively, and the assumption that the scattered amplitude must vanish cannot be fully substantiated by the results of this investigation.[2]

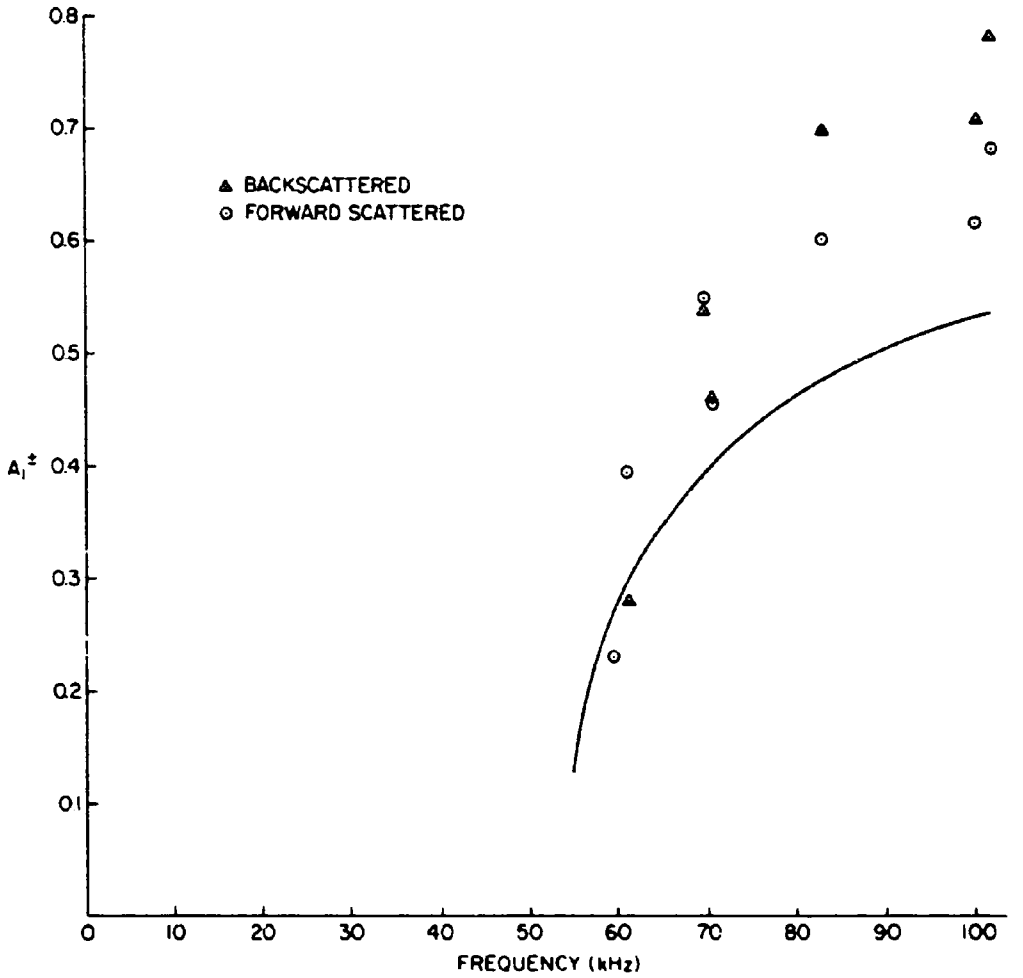

Figure 4-8. First Scattered Order Amplitude $A_1^{\pm}$ for $\theta_i = 0^{\circ}$

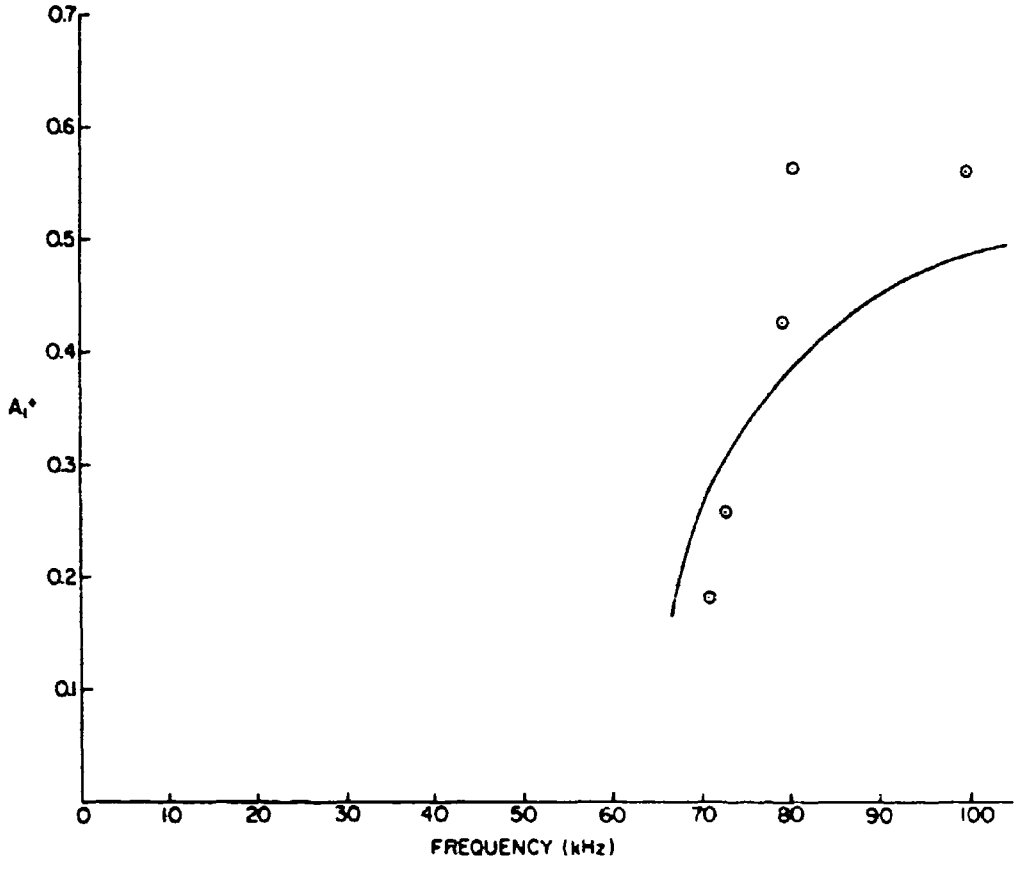

Figure 4-9. First Forward Scattered Order Amplitude A_1^+ for $\theta_i = 10^\circ$

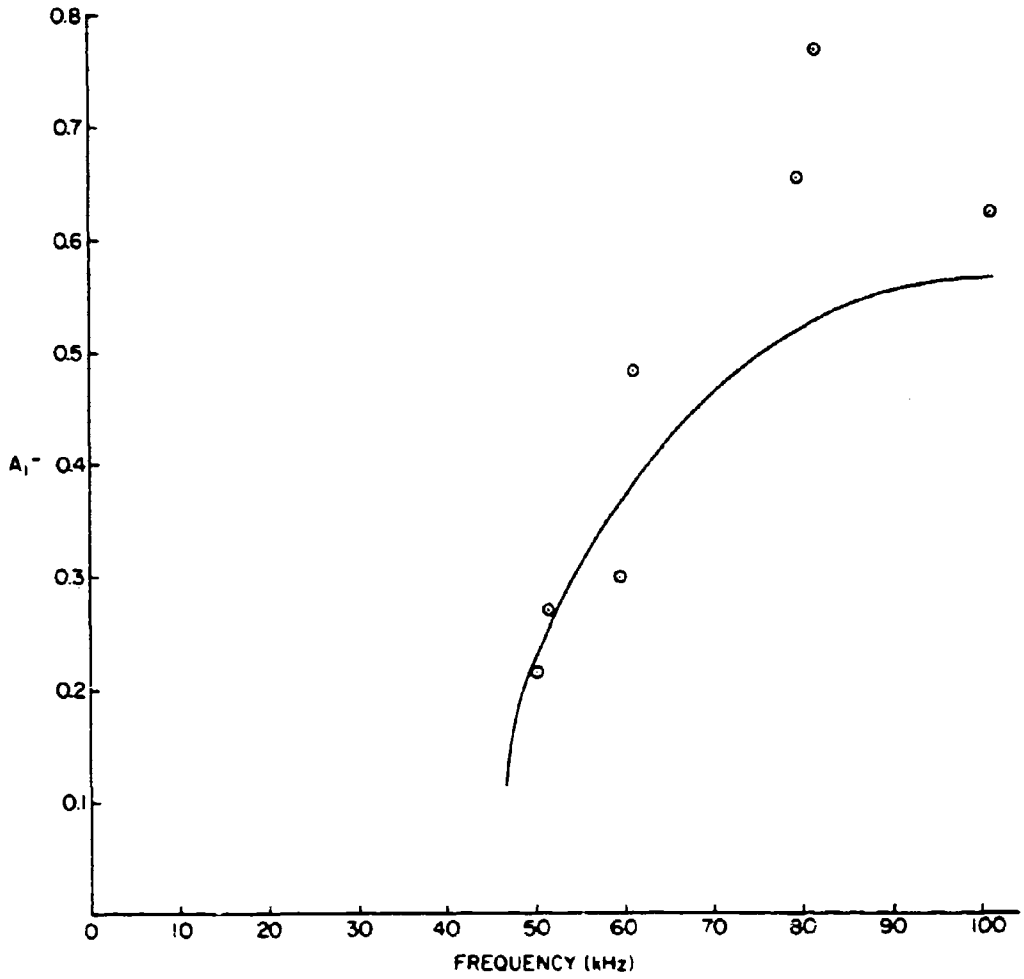

Figure 4-10. First Backscattered Order Amplitude A_1^- for $\theta_i = 10^\circ$

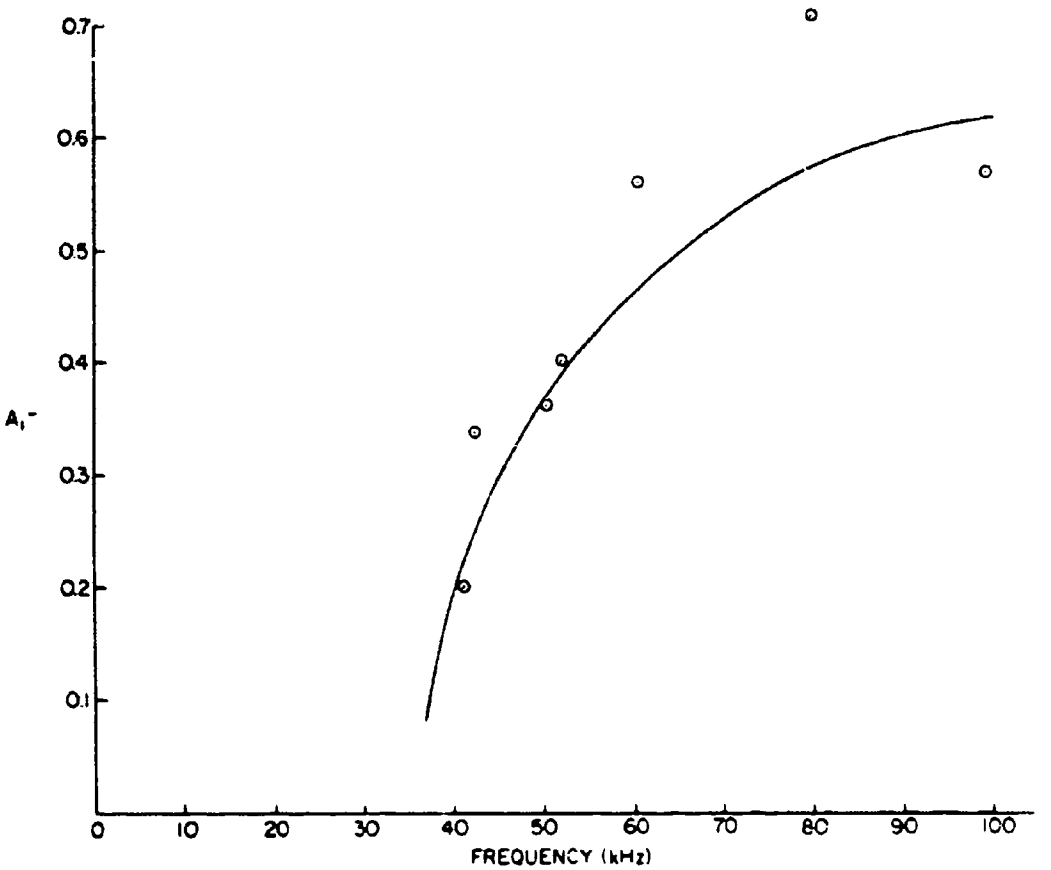

Figure 4-11. First Backscattered Order Amplitude A_1^- for $\theta_1 = 30^\circ$

4.2.3 Second Scattered Order Amplitudes. Agreement between theory and experiment for the second backscattered order is much poorer than for the first (Figures 4-12 and 4-13). Because the second forward scattered order was below cut-off for the frequencies used, it could not be measured. Again, the value of the scattered amplitude at cut-off is unclear, even more so than for the first order. Apparently, the Eckart theory of scattering tends to become more inaccurate for the higher orders, especially as the angle of incidence becomes large (Figure 4-12).

However, Figure 4-12 indicates that for a 10° angle of incidence, values of A_2^- less than 0.1 could be measured. It is difficult to explain how such a small value could be attained in view of the constancy of the experimental cut-off values obtained in all other areas of the investigation. Experimental error in this case seems rather unlikely, in that two separate trials produced nearly identical results.

Figure 4-14 shows the measured relative spatial amplitude level for a fixed acoustic frequency when a time dependent random surface was the scatterer. The graph for 60kHz

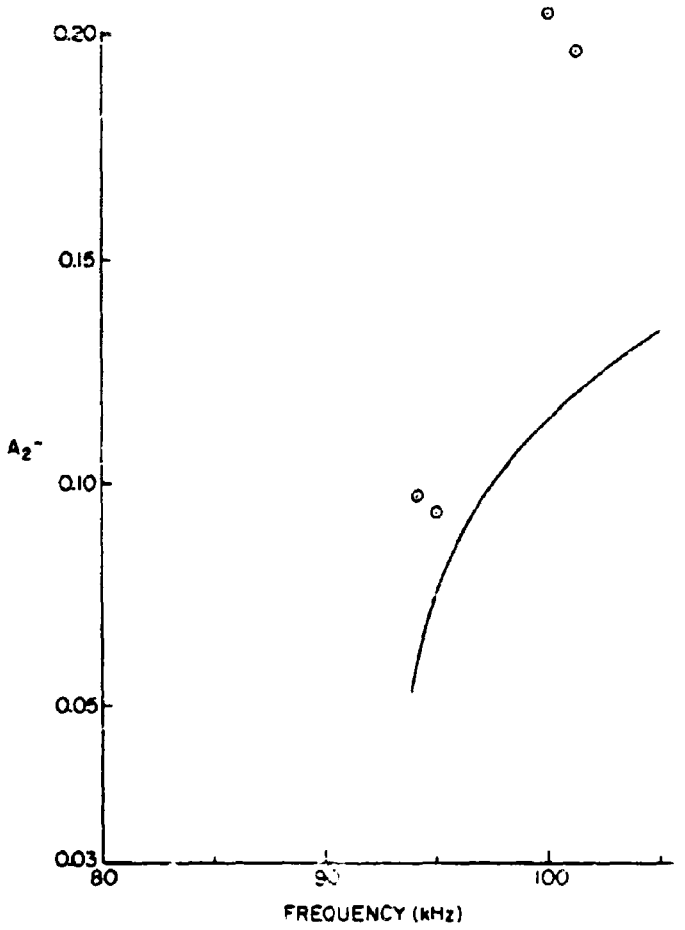

Figure 4-12. Second Backscattered Order Amplitude A_2^- for $\theta_1 = 10^\circ$

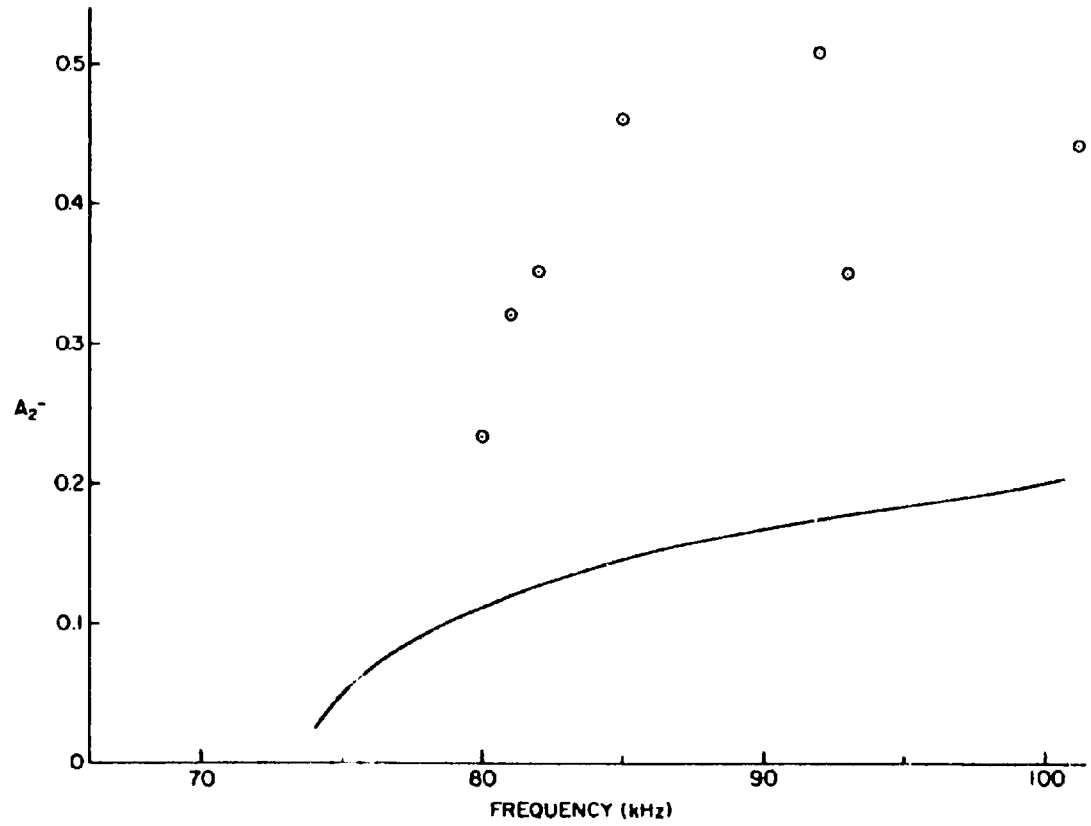

Figure 4-13. Second Backscattered Order Amplitude A_2^- for $\theta_i = 30^\circ$

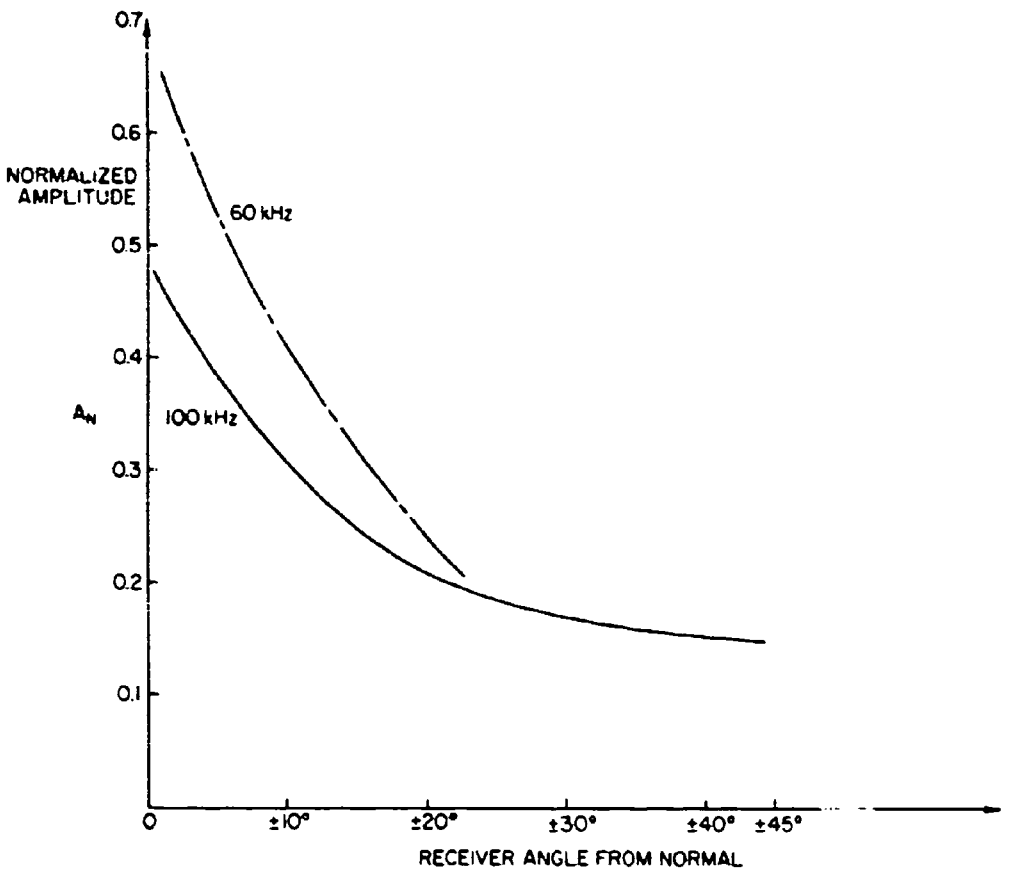

Figure 4-14. Normalized Scattered Amplitude A_n for a Random Surface for $\theta_i = 0^\circ$

is more strongly peaked in the specular direction than for 100kHz, indicating that the surface scatters more diffusely at the higher frequencies. Finally, the observed scattered amplitudes reveal symmetric behavior for both forward and backscattered directions.

4.3 Internal Structure of Correlation Function

The internal structure of the envelope of the correlation function for various experimental configurations was examined and found in general agreement with calculation. The correlation length, λ_c, was usually found to be different from the acoustic wavelength, λ. The receiver, in traversing the tank cut obliquely across the direction of propagation of the scattered order; thus, the receiver recorded a projection of the actual acoustic wavelength. Mathematically, the relationship between λ_c and λ is expressed as:

$$\lambda_c = \lambda/\sin\theta_i \qquad \text{for specular reflections,} \quad (4.6)$$

$$\lambda_c = \lambda/\cos\delta_j^{\pm} \qquad \text{for scattered orders,} \quad (4.7)$$

where Equation (4.1) relates $\delta_j^{\pm}$ and λ.

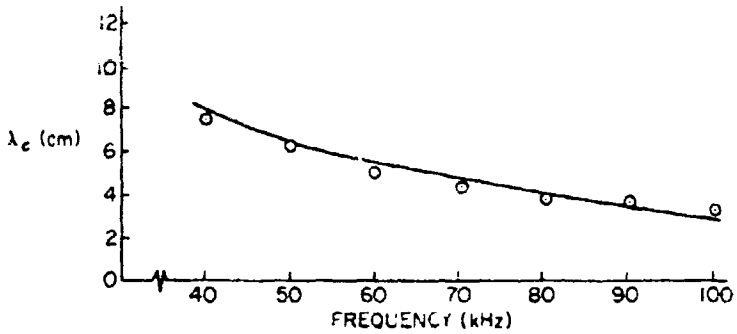

Figure 4-15. Specular Correlation Length λ_c for $\theta_i = 30^\circ$

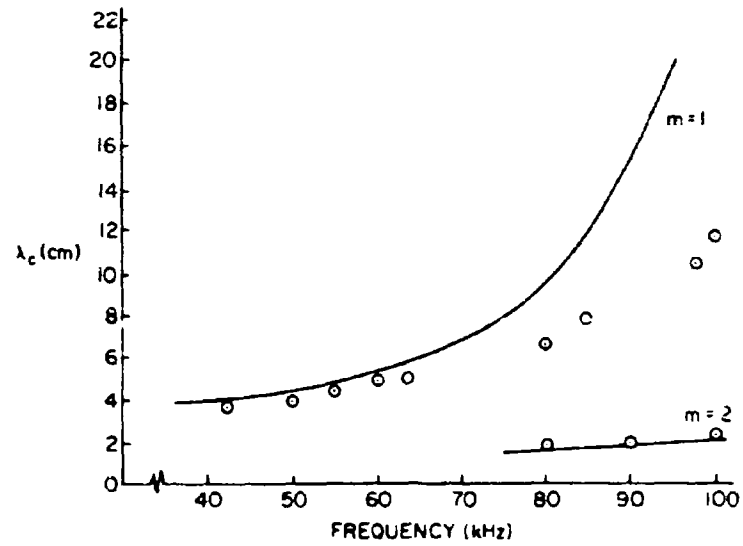

Figure 4-16. First (m=1) and Second (m=2) Backscattered Order Correlation Length λ_c for $\theta_i = 30^\circ$

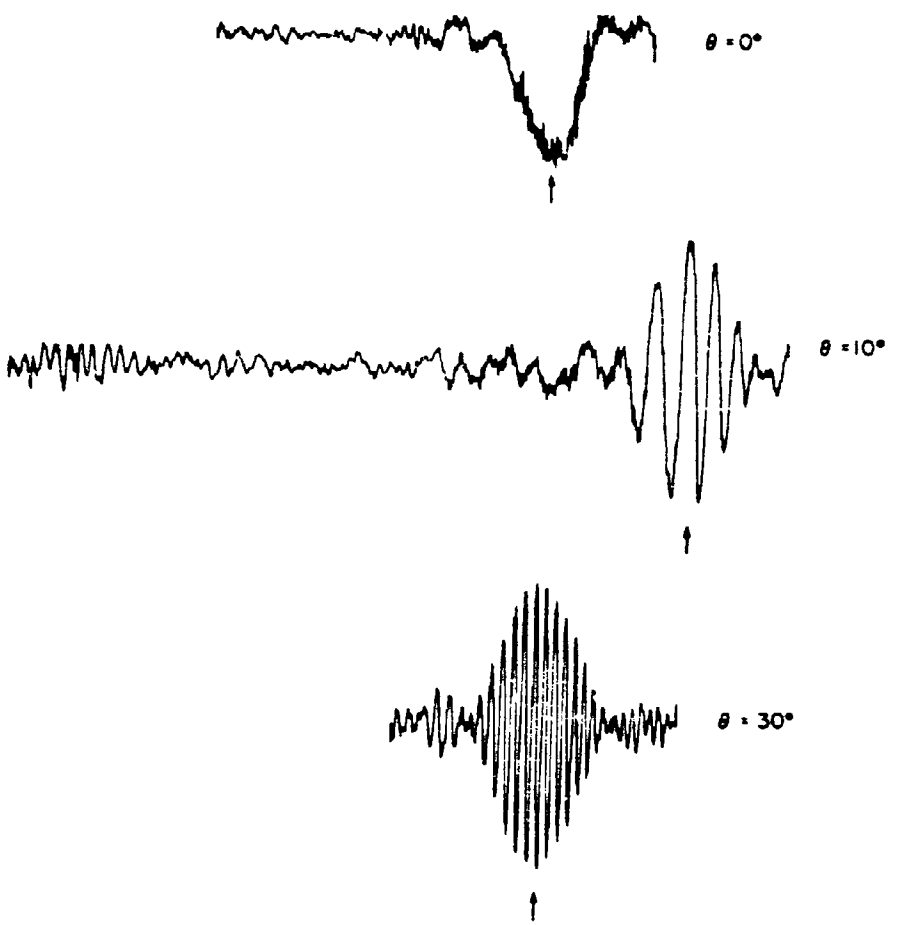

Figure 4-17. Specular Reflection Correlation Length vs Angle of Incidence

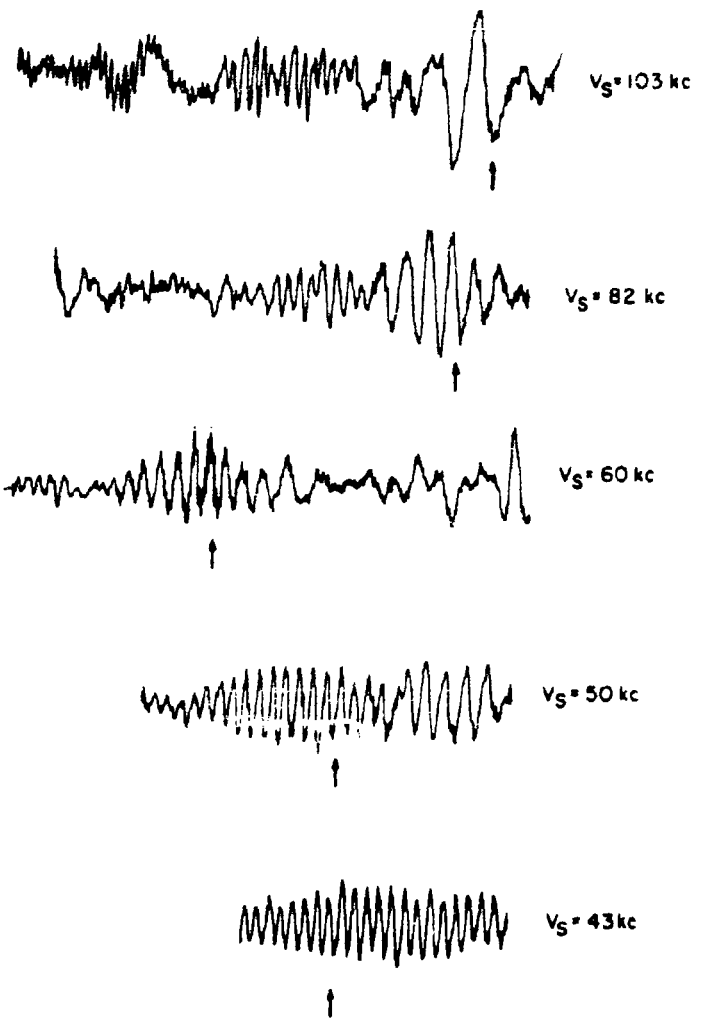

Figure 4-18. First Backscattered Order Correlation Length Variation

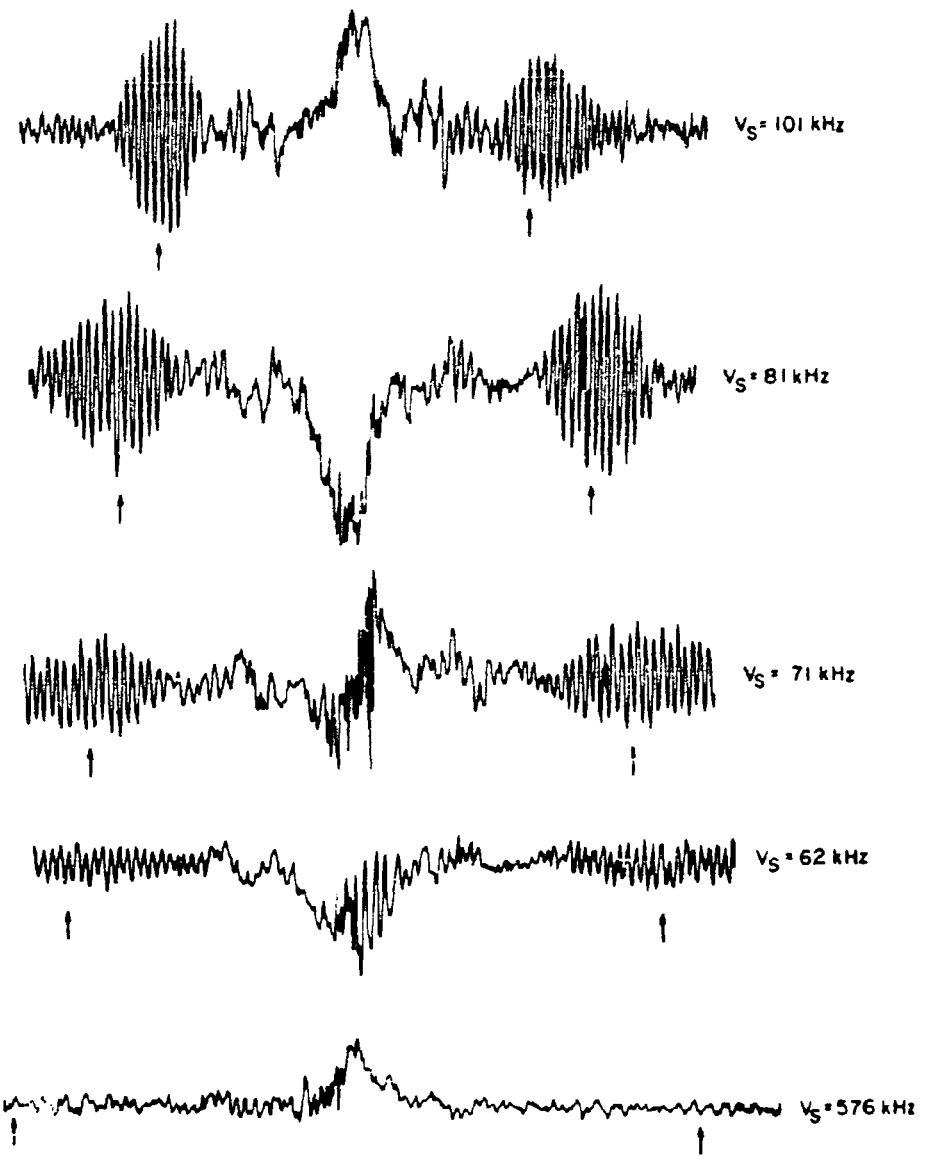

Figure 4-19. First Scattered Order Cut-Off Sequence for $\theta_i = 0^\circ$

Figures 4-15 and 4-16 present a comparison between typical experimental results and Equations (4.6) and (4.7). These equations afforded another means of determining the identity of a particular scattered order. The specular correlation length, λ_c, displayed consistently good agreement with Equation (4.6) for all incident angles used, including $\theta_i = 0$. In the case of normal incidence ($\theta_i = 0$), only a single peak of the correlation function was obtained, suggesting λ_c was infinite (Figure 4-17).

For scattered amplitudes, however, Equation (4.7) became more inaccurate as δ_j^+ approached 90° (Figure 4-16). It is not presently understood why these equations are valid for specular reflections, but not for scattered orders. Near cut-off, however, there was good agreement with the theory in all cases, as λ_c approached λ.

CHAPTER V

SUMMARY

5.1 The Problem and Its Significance

During the past twenty years, scientists have investigated scattering from pressure release sinusoidally corrugated surfaces using sound pulses. In the present study, the scattered pressure amplitudes were measured for the case of a continuous source using a variable level correlator to separate the scattered signal from the background noise. This technique was applied in the cut-off frequency region of the first two scattered orders and the results then compared to Eckart's theory of scattering. The present investigation establishes an alternate approach to measuring a scattered sound field and contributes further proof of the validity of existing scattering theory.

5.2 Experimental Procedure

The scattered amplitudes were always referenced to the amplitude that would be reflected by a plane pressure release surface. For a given angle of incidence, the scattered

amplitude was measured along a portion of an arc of a circle, centered about the midpoint of the corrugation. Consequently, inverse spreading and transit time were the same for all paths propagating from the center. The grating equation was then used to calculate the arc positions for the reception of a spectrum of a given order and frequency. Traversing the tank at the appropriate depth to intercept the calculated point produced a graph of a spatial correlation function on the x-y recorder. The best graph was selected after considering the position and magnitude of the maximum of the correlation function and the shape of the function's envelope.

After replacing the corrugated surface by a plane surface, a similar recording was made under identical conditions for the specularly reflected amplitude. By utilizing the input-output calibration curve of the correlator system, a method was derived to relate mathematically the measured correlation amplitudes to the "relative" amplitudes.

5.3 Results and Conclusions

With the technique described, results were obtained for the specular and the first two scattered order amplitudes at three angles of source incidence. A comparison with theory

revealed that best agreement existed for the specular amplitudes, and poorest for the second scattered order amplitudes. This result is not very surprising, since several assumptions of the theory were violated. Because the higher order terms of the solution represent the higher scattered orders, the scattered orders would be expected to suffer most by the inaccuracies of the theory. The scattered amplitudes agreed best with theory for frequencies just above cut-off. For the second scattered order, the results obtained for small angles of incidence agreed better with theory than those for large angles; in contrast, agreement for the first order spectra with theory depended little on angle of incidence. The cut-off of the scattered amplitudes occurred consistently at slightly higher frequencies than calculated. In all instances, extinction of the scattered amplitudes below cut-off was inferred from the large positive slope of the scattered amplitude just above cut-off and the negative results obtained at frequencies below cut-off. The magnitude of the scattered amplitude at cut-off could not accurately be determined probably due to the limited signal resolving capability of the correlator. Finally, the internal structure of the correlation function envelope showed good agreement with theory, except as the direction of the scattered order approached the normal to the surface.

5.4 Suggestions for Further Investigation

Another study is required to determine the exact cut-off amplitude. To succeed, the correlator system requires a higher signal resolving capability than was available here. Furthermore, utilizing higher incident angles would facilitate measuring the cut-off amplitude of forward scattered orders, since these cut-off amplitudes should theoretically be larger at higher angles of incidence. Investigation of the scattering process from random surfaces using the variable level correlator is suggested in light of the success achieved in the present application. Use of other continuous source generators would provide a means of comparing different scattered signals.

BIBLIOGRAPHY

1. Bernard, G., et. al., "Underwater-Sound Reflections from a Pressure-Release Sinusoidal Surface," J. Acoust. Soc. Am. 39, 1162-1169 (1966).

2. Beckmann, P. and A. Spizzichino, The Scattering of Electro-magnetic Waves from Rough Surfaces, (Pergamon Press, Ltd., London, 1963), Chapters 1-4.

3. Brekhovskikh, L.M., "Wave Diffraction by an Uneven Surface," Soviet Physics - JETP 23, 275-289 (1952).

4. Copson, E.T. and B.B. Baker, The Mathematical Theory of Huygens Principle, (The Clarendon Press, Oxford, England, 1950), Chapter I.

5. Davio, Marc, "Variable Level Correlators," Proceedings of NATO-Marina Italiana Advanced Study Institute of Stochastic Problems in Underwater Sound Propagation, Lerici, Italy, Sept. 18-23, 1967.

6. Eckart, C., "The Scattering of Sound from the Sea Surface," J. Acoust. Soc. Am. 25, 566-570 (1953).

7. Horton, C. and T. Muir, "Theoretical Studies on the Scattering of Acoustic Waves from a Rough Surface," J. Acoust. Soc. Am. 41, 627-634 (1967).

8. Jackson, D., Classical Electrodynamics, (John Wiley and Sons, Inc., New York, 1965), 280-283.

9. Kinsler, L., and A. Frey, Fundamentals of Acoustics, (John Wiley and Sons, Inc., New York, 1962), 166-177.

10. LaCasce, E.O., and P. Tamarkin, "Underwater Sound Reflection from a Corrugated Surface," J. Appl. Phys. 27, 138-148 (1956).

11. Leporskii, A.M., "Experimental Investigation of Diffraction of Acoustic Waves by Periodic Structures," Soviet Phys. Acoust. 2, 50-59 (1956).

12. Macaluso, John, Private Communication.

13. Marsh, H.W., "Exact Solution of Waves Scattering by Irregular Surfaces," J. Acoust. Soc. Am. 33, 330-333 (1961).

14. Mintzer, D., "Discussion of the Paper by C. Eckart on Sea Surface Scattering," J. Acoust. Soc. Am. 25, 1015 (L) (1953).

15. Proud, J.M., "Reflection of Sound From a Saw-Tooth Profile," Tamarkin, and Mecham, W.C. J. Appl. Phys. 28, 1298-1301 (1957).

16. Lord Rayleigh, Theory of Sound, (Dover Publications, New York, 1945), Vol. 2, 89-96.

17. Skudrzyk, Eugen, Die Grundlagen der Akustik, (Springer-Verlag, Vienna, 1954).

18. Tolstoy, Ivan, and C.S. Clay, Ocean Acoustics; Theory and Experiment in Underwater Sound, (McGraw-Hill Book Company, New York, 1966), 189-202.

19. Uretsky, J.L., "Reflection of a Plane Sound from a Sinusoidal Surface," J. Acoust. Soc. Am. 35, 1293-1294 (1963).

20. Uretsky, J.L., "The Scattering of Plane Waves from Periodic Surfaces," Am. Phys. 33, 400-427 (1965).

APPENDIX A

SOURCE AND RECEIVER DISTANCE APPROXIMATIONS

A. Utilizing Figure A-1, we have

$$r_o = [\,(x_1 + x_o)^2 + (\zeta - Z_o)^2\,]^{1/2}$$

$$= (\,r_{oo}^2 + x_1^2 + \zeta^2 + 2x_1 x_o - 2\zeta Z_o)^{1/2}$$

since, $(x_o^2 + Z_o^2) = r_{oo}^2$

$$= r_{oo}\,(1 + x_1^2/r_{oo}^2 + \zeta^2/r_{oo}^2 + 2x_o/r_{oo}^2 - 2\zeta Z_c/r_{oo}^2\,)^{1/2} \qquad \text{(A-1)}$$

After applying the Binomial expansion and dropping second order terms,

$$r_o \cong r_{oo}\,[\,1 + (x_o/r_{oo})\,x_1/r_{oo} - (Z_o/r_{oo})\,\zeta/r_{oo} + \ldots\,]$$

$$r_o \simeq (r_{oo} + x_1 \sin\delta_1 - \zeta\cos\delta_1)$$

however,

$$\delta_1 = (\delta_2 - \pi/2) \qquad \text{(A-2)}$$

hence, $\sin\delta_1 = -\cos\delta_2$

and $(1-C_o^2)^{1/2} = -a_o$

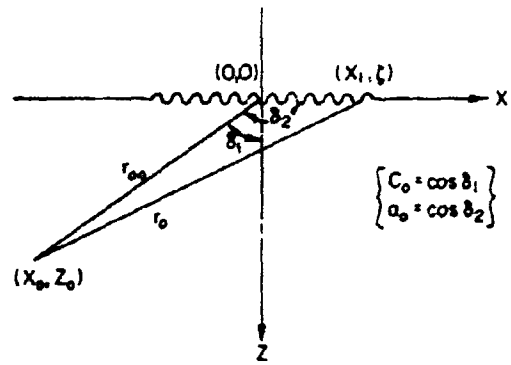

Figure A-1. Source Distance Approximation

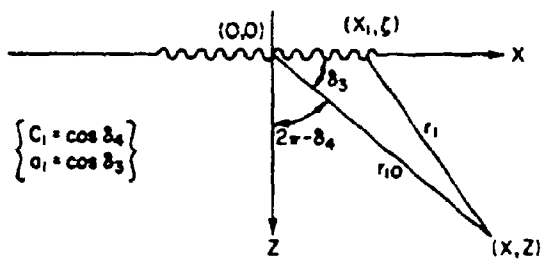

Figure A-2. Receiver Distance Approximation

With these substitutions, (A-2) becomes

$$r_o \simeq r_{oo} - (a_o X_1 + c_o \zeta) \qquad (A-3)$$

B. To find an approximation for the receiver distance, we proceed similarly. From Figure A-2,

$$r_1 = [\ (x_1 - x)^2 + (\zeta - z)^2\ ]^{1/2} \qquad (A-4)$$

$$= [\ r_{10}^2 + X_1^2 + \zeta^2 - 2xx_1 - 2\zeta z\ ]^{1/2}$$

since, $(x^2 + z^2) = r_{10}^2$

or $$r_1 = r_{10}\ [\ 1 + (x_1/r_{10})^2 + (\zeta/r_{10})^2 - 2xx_1/r_{10}^2 - 2\zeta z/r_{10}^2\ ]^{1/2}$$

Applying the Binomial expansion and dropping second order terms again,

$$r_1 \simeq r_{10}\ [\ 1 - (x/r_{10})\ x_1/r_{10} - (z/r_{10})\ \zeta/r_{10} + \ldots\ ]$$

$$\simeq r_{10} - x_1 \cos\delta_3 - \zeta \sin\delta_3 \qquad (A-5)$$

but $\sin\delta_3 = \cos(2\pi - \delta_4)$

$= \cos\delta_4$

$= c_1$

With this substitution (A-5) becomes

$$r_1 \simeq r_{10} - (a_1 X_1 + c_1 \zeta)$$

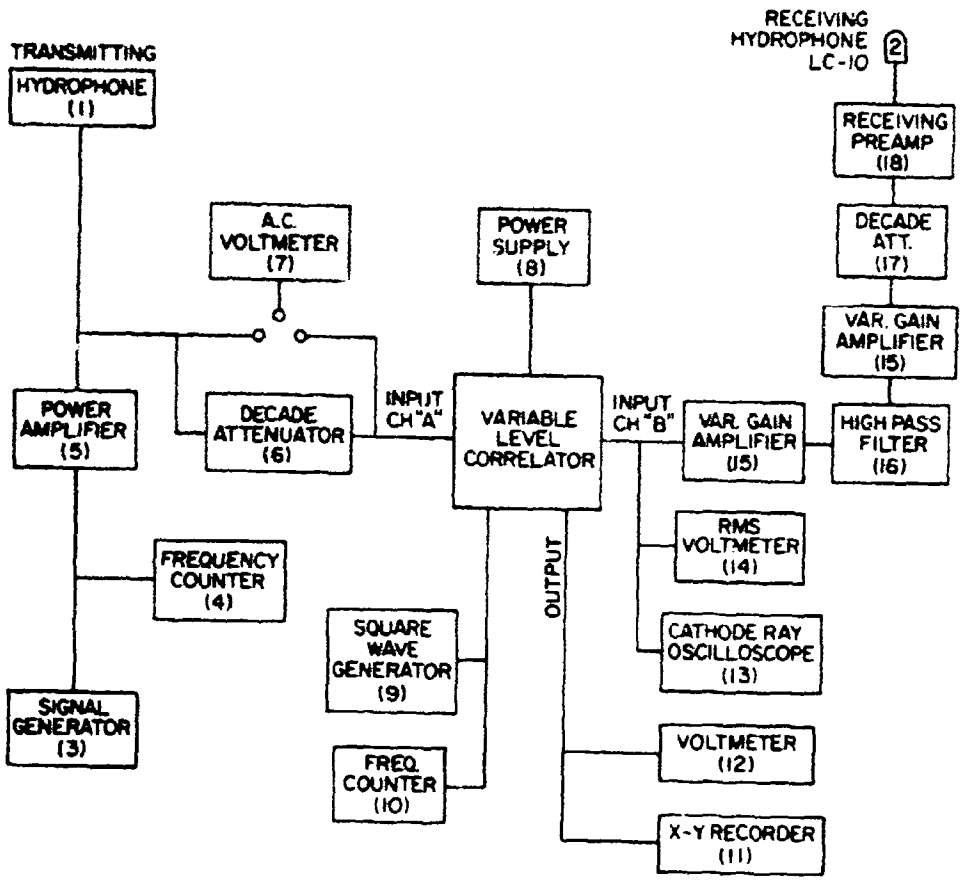

Figure B-1. Correlator System Component Schematic

CORRELATOR SYSTEM COMPONENTS

(1) USRD TYPE F-33 TRANSMITTING HYDROPHONE (See Appendix C).

(2) LC-10 RECEIVING HYDROPHONE (Atlantic Research) (See Appendix D).

(3) BEAT FREQUENCY OSCILLATOR, TYPE 1013 (Brüel and Kjaer).

(4) ELECTRONIC COUNTER, MODEL 5512A (Hewlett-Packard).

(5) POWER AMPLIFIER-200W, TYPE K-107 (McIntosh).

(6) ATTENUATOR SET, 340D (Hewlett-Packard).

(7) A. C. VOLTMETER, MODEL 310A (Ballantine Laboratories, Inc.).

(8) POWER SUPPLY (+6V, +12V, -18V), MODEL RP-32 (Computer Control Company).

(9) SQUARE WAVE GENERATOR (3 n sec RISE TIME), TYPE 107 (Tektronix).

(10) UNIVERSAL EPUT AND TIMER, MODEL 7360 (Beckmann).

(11) MOSELEY X-Y RECORDER, 7035B (Hewlett-Packard).

(12) PRECISION A.C. - D.C. VOLTMETER, MODEL AC-150B-1 (Calibration Standards Corp.).

(13) OSCILLOSCOPE, TYPE 321A (Tektronix).

(14) TRUE RMS VTVM, MODEL 320A (Ballantine Laboratories, Inc.).

(15) VARIABLE GAIN AMPLIFIER 0-50dB GAIN WITH 10dB STEPS.

(16) HIGH PASS FILTER (low frequency cut-off at 2kHz).

(17) DECADE ATTENUATOR, TYPE NO 1450-TA (General Radio).

(18) RECEIVING PREAMPLIFIER.

APPENDIX C

TRANSMITTING HYDROPHONE SPECIFICATIONS

30 November 1966

Preliminary Operating Instructions

USRD TYPE F33 TRANSDUCER
Serial 7

1. GENERAL DESCRIPTION

The USRD type F33 transducer was designed as a general purpose unidirectional transducer for use in calibration measurements in the frequency range 1 to 150kHz.

The sensitive element consists of two piezoelectric ceramic arrays mounted coaxially. The smaller, inner array is composed of twelve 0.5-in.-dia by 0.10-in.-thick lead zirconate - lead titanate elements cemented to Kennametal disks. This array is approximately 1.5 in. wide and 2 in. high; it is useful in the frequency range 5 to 150kHz.

The larger array is constructed from 64 modified barium titanate ceramic plates 1 in. long by 0.75 in. wide by 0.250 in. thick. Each plate is cemented to a steel backing plate embedded in butyl rubber to form an array approximately 8 in. wide by 8.5 in. high. When the two arrays are driven simultaneously, the transducer is useful in the frequency range 1 to 50kHz. Normally, the transducer is calibrated unbalanced, with the shield and the low-output lead connected to ground.

The transducer is provided with 100 ft. of vinyl-sheathed cable. The leads to each array section are individually shielded; a 1-ft. length of cable provided with mating connectors serves to connect the inner and the outer sections in parallel. The entire transducer then can be driven by a signal applied to pins A and B of the AN adapter. The shields are accessible at pin E.

2. SPECIFICATIONS

Frequency range:	both section, 1 to 50kHz inner section, 5 to 150kHz
Maximum hydrostatic pressure:	500 psig
Operating temperature range:	0 to 35°C
Maximum input:	200 V rms
Nominal capacitance at end of cable:	outer section, 54,500 pF inner section, 12,000 pF both sections, 66,500 pF
D-c resistance:	greater than 1000 M
Over-all dimensions:	diameter, 10.75 in. case depth, 1.75 in. acoustic center to top mounting bracket, 11.62 in.
Weight with 100-ft cable:	38 lb

3. DIRECTIVITY

With both sections operating, the total beam width at the 3-dB down points is 7.5 degrees at 50kHz. The minor lobes are down at least 14dB with respect to the major lobe. When only the inner section is used, the total beam width at 150kHz is 12 degrees.

4. TEMPERATURE AND HYDROSTATIC PRESSURE - RESPONSE CHARACTERISTICS

No significant changes have been observed in the operating characteristics at hydrostatic pressures to 500 psi and temperatures between 5 and 30°C.

5. PREPARATION OF THE TRANSDUCER FOR USE

Attach a fixture to the mounting bracket provided. Do not support the transducer by the cable. To remove air bubbles as completely as possible and thus avoid erroneous results, wash the entire transducer with a wetting agent at the time that it is lowered into the water.

6. CAUTIONS

This transducer is a calibrated standard and should be handled with care. Avoid sharp blows and punctures to the rubber acoustic window and the cable sheath. Store in the carrying case when not in use.

APPENDIX D

RECEIVING HYDROPHONE SPECIFICATIONS

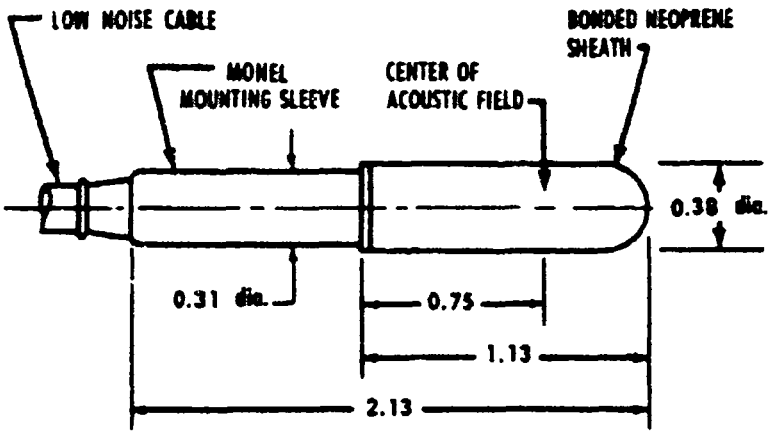

Figure D-1. LC-10 Hydrophone

NOMINAL CHARACTERISTICS

	UNITS	VALUES
Voltage Sensitivity (CW)	V/psi	0.3
Ref 1 V/μbar	dB	-108
Capacitance with 25-ft Cable	pF	7500
Useful Frequency Range	Hz	0.1 to 120,000
D.C. Resistance (min)	MΩ	1000
Maximum Static Pressure	psi	5000
Directivity, Horizontal, 100 kHz	±dB	1
Directivity, Vertical, 25 kHz	±dB	2
Operating Temperature Range	°C	-60 to +100
Thermal Sensitivity	dB/°C	0.03
Total Weight with 25-ft Cable	oz	10
Sensing Element		Lead Zirconate Titanate